BV

LPC CAEN

LABORATOIRE DE PHYSIQUE CORPUSCULAIRE

ISMRA - Boulevard Maréchal Juin - 14050 CAEN CEDEX - FRANCE

CERN LIBRARIES, GENEVA
SCAN-9505170

SW9522

Binary dissipative processes and formation of hot nuclei in $^{36}Ar + ^{27}Al$ reactions from 55 to 95 MeV/u

J. Péter, S.C. Jeong, J.C. Angélique, G. Auger, G. Bizard, R. Brou, A. Buta, C. Cabot, Y. Cassagnou, E. Crema, D. Cussol, D. Durand, Y. El Masri, P. Eudes, Z.Y. He, A. Kerambrun, C. Lebrun, R. Legrain, J.P. Patry, A. Péghaire, R. Régimbart, E. Rosato, F. Saint-Laurent, J.C. Steckmeyer, B. Tamain, E. Vient

May 1995 LPCC 95-10

Submitted to Nuclear Physics A

INSTITUT NATIONAL
DE PHYSIQUE NUCLEAIRE ET DE PHYSIQUE DES PARTICULES

CENTRE NATIONAL DE LA RECHERCHE SCIENTIFIQUE

INSTITUT DES SCIENCES
DE LA MATIERE ET DU RAYONNEMENT

UNIVERSITÉ DE CAEN

Téléphone : 31 45 25 00
Télécopie : 31 45 25 49

BINARY DISSIPATIVE PROCESSES AND FORMATION OF HOT NUCLEI IN $^{36}Ar + ^{27}Al$ REACTIONS FROM 55 TO 95 MeV/u

J. Péter [1], S.C. Jeong [1,7-d], J.C. Angélique [1], G. Auger [2], G. Bizard [1], R. Brou [1], A. Buta [1-a], C. Cabot [2-c], Y. Cassagnou [8], E. Crema [2-b], D. Cussol [1], D. Durand [1], Y. El Masri [3], P. Eudes [4], Z.Y. He [6], A. Kerambrun [1], C. Lebrun [4], R. Legrain [8], J.P. Patry [1], A. Péghaire [2], R. Régimbart [1], E. Rosato [5], F. Saint-Laurent [2], J.C. Steckmeyer [1], B. Tamain [1], E. Vient [1]

1) LPC Caen, IN2P3-CNRS, ISMRA and University of Caen, 14050 CAEN, FRANCE
2) GANIL, BP 5027, 14021 CAEN CEDEX, FRANCE
3) Institut de Physique Nucléaire, UCL, 1348 LOUVAIN-LA-NEUVE, BELGIUM
4) SUBATECH, Université et Ecole des Mines de Nantes, IN2P3-CNRS 44072 NANTES, FRANCE
5) Dipartimento di Scienze Fisiche and INFN, Univ. di Napoli, 80125 NAPOLI, ITALY
6) Institute of Modern Physics, LANZHOU 730000, CHINA
7) Department of Physics, Soongsil University, SEOUL, KOREA
8) DAPNIA/SPhN, CEN Saclay, FRANCE
a) Permanent address : I.F.A., Heavy Ion Department, BUCHAREST, ROMANIA
b) Permanent address : Inst. di Fisica, Univ. de SAO PAULO, BRAZIL
c) On leave of absence from IPN ORSAY, France
d) Present address : Institute of Nuclear Studies, University of TOKYO, JAPAN

Abstract : A 4 π multidetector array with a high efficiency has been used to detect the charged products from reactions induced by ^{36}Ar on ^{27}Al at energies ranging from 55 to 95 MeV/u. Well characterized events were selected and sorted as a function of the impact parameter. Fusion or full stopping events have a very small cross section. Dissipative binary collisions accompanied by pre-equilibrium emission were found to dominate for all impact parameters. The mass of the quasi-projectile has been reconstructed from its products and found to be slightly below the projectile mass. Isotropic emission in its rest frame has been observed at all energies and impact parameters, indicating that equilibrated nuclei may have been formed. The excitation energy of the quasi-projectile, determined via calorimetry, and the slope of kinetic energy spectra of α-particles were found to increase with incident energy and with decreasing impact parameter. E*/A values above 11 MeV are reached in a sizable cross section (70 mb). The mass distribution and kinetic energy spectra of emitted particles and fragments are essentially governed by the excitation energy, with a weak dependence on the impact parameter. The evolution of dissipative processes from deep inelastic collisions to the participant-spectator regime is discussed.

1. Introduction :

Hot nuclei can be formed in nucleus-nucleus collisions at intermediate energies [1]. One of the open questions in the study of such systems is the amount of energy which has been thermalized. This is obtained by determining the mass A, the excitation energy E^* and the temperature T of the system. Since these quantities vary as a function of the violence of the collision, the experimental data must be sorted according to this quantity. In inclusive experiments, only a rough sorting is possible. Moreover, the excitation energies and temperatures derived from these measurements rely heavily on the reaction mechanism (e.g. incomplete fusion or massive transfer from the light nucleus to the heavy one) assumed to be responsible for the formation of the hot nuclei.

In order to study the decay of hot nuclei in a reaction, one must first determine the number of hot nuclei which are formed after the first step of the collision (emission of pre-equilibrium nucleons and clusters from the interaction zone). This is related to the collision dynamics. In peripheral collisions, there is always one quasi-projectile nucleus (fast source) and one quasi-target nucleus (slow source). For asymmetric systems, incomplete fusion occurs at least in central and semi-central collisions [1]. In central collisions, for all but heavy systems the evolution is from a very large cross section for complete fusion at low energy to a very small cross section for full stopping at high energies [2]. At high energies, over almost the whole range of impact parameters, two excited "spectators" are left after emission of participant nucleons from the interaction region. At intermediate energies (20 to 100 MeV/u), incomplete fusion, massive transfer mechanisms and deep inelastic collisions have been invoked to explain the observed distributions of products, especially for heavy residues. The energies at which fusion dynamics are replaced by binary reaction dynamics remains an open question since most experimental data to date have been obtained from inclusive measurements. Three sources of particles have been observed : near the projectile rapidity, at small rapidity and at mid-rapidity. 4π multidetector arrays make it possible to detect most of the charged final products and to reconstruct the excited primary products on an event-by-event basis. In very asymmetric systems, the slow source has been shown to be consistent with incomplete fusion between the heavy nucleus and part of the light one. In symmetric or nearly symmetric systems, the situation is not clear. For very heavy systems, fusion does not occur at energies below 20 MeV/u, even in central collisions. For $^{129}Xe+^{nat}Ag$, ^{197}Au collisions at 23.7 and 27 MeV/u, the overall trends of inclusive data can be explained by binary processes (modified participant-spectator model or extended deep inelastic model) [3]. 4π measurements performed for the heavy systems $^{209}Bi+^{136}Xe$ [4] and Pb+Au [5] indicate that the binary character persists at 28-29 MeV/u for the most dissipative (central) collisions. For systems which undergo

fusion below 10 MeV/u, strong indications of a binary behavior for Ar+Ag collisions above 25 MeV/u were found [6].

The disappearance of evaporation residues in the Ar+Al system at 19.7 MeV/u was interpreted as being due to the sequential decay of the compound nuclei rather than to the vanishing of fusion-like products [8]. Ref. 9 showed that composite nucleus formation vanishes above 27 MeV/u, which was tentatively attributed to a temperature limit of the composite nucleus. At 44 and 60 MeV/u, the correlation between the projectile-like and the target-like fragments formed in peripheral interactions was measured and explained by an extended version of the abrasion-ablation model or by the equal sharing of excitation energy between the two nuclei [10].

The formation of hot nuclei raises a number of questions. Is a part of the excitation energy in form of collective energy instead of thermal energy ? How do the nuclei decay ? At low excitation energies, the standard decay is the sequential statistical emission of particles and clusters (evaporation or fission). When the incident energy increases, the probability of emission of heavier clusters (Intermediate Mass Fragments, IMF's) increases, and multiframent events become a significant fraction of the reaction cross section. Are these multifragment events due to the continuation of sequential binary decay or to a fast multifragmentation process ? Is this process related to the presence of compressional energy ? Many papers have been published on the question of multifragmentation [11].

In this paper, we will present the results of experimental measurements with a 4π detector which provided an almost complete detection of the final charged products (at least the products from one of the two hot nuclei formed). An event-by-event analysis made it possible to extract various characteristics. In section 2, the experimental set-up is described. In such studies, it is essential to avoid contamination of the data by poorly measured events. The method used to check the quality of each recorded event is described in section 3. Since the mass and excitation energy of the nuclei can vary strongly as a function of the violence of the collision, a meaningful full sorting must be used. The sorting of the well characterized events as a function of the impact parameter is described in section 4. In section 5 the analysis of experimental data leads to an upper limit of the incomplete fusion cross section. After pre-equilibrium emission, a quasi-target (slow source) and a quasi-projectile (fast source) remain. The characteristics of the quasi-projectile are shown in section 6 (mass, thermal equilibrium, excitation energy) while its decay is studied in section 7 (apparent temperature, charge distribution of the final products).

We have performed previously similar measurements for the reaction $^{40}Ar + ^{27}Al$ at energies ranging from 25 to 65 MeV/u [12]. We present here the results of measurements of the $^{36}Ar + ^{27}Al$ system at incident energies of 55, 67, 79, 86 and 95 MeV/u. Beyond the higher energies employed in the present study, an important feature is the use of ^{36}Ar instead of ^{40}Ar. The number of emitted neutrons - which are not detected - is therefore reduced and a larger proportion of the emitted particles is detected. In addition, the experimental set-up and the analysis method have been improved, as explained in section 2.

2. Experimental set-up :

The experiments were performed at the GANIL facility in the reaction chamber Nautilus. Charged products were detected in a nearly 4π geometry using the two complementary multidetector systems MUR [14] and TONNEAU [15] (fig. 1). The forward angles between 3.2° and 30° were covered by a wall of 96 plastic scintillators arranged in 7 concentric rings located 210 cm from the target. Angles between 30° and 150° were covered by a spherical barrel which was located 80 cm from the target (30° to 90° in ref. 12). The main improvement relative to ref. 12 was the addition of 7 large solid angle silicon telescopes installed 60 cm from the target and at polar angles from 3° to 30° and an azimuthal range of 22°. These telescopes detected fragments with charges ≥ 3 and were used for those events which had fragment with a charge above 8. The overall geometrical efficiency of the array was 80 % . To reduce the number of electrons emitted from the target, a positive high voltage of 45 kV was applied to the target. As an additionnal precaution, aluminum foils 68 μm thick covered the scintillators. Due to these foils no detectable signal was produced for protons and α-particles having velocities below 2.5 cm/ns (3.2 MeV/u). This detection threshold increases with the charge, reaching 3.2 cm/ns (5.3 MeV/u) for ^{16}O. These thresholds are lower than in previous experiments with ^{40}Ar where 200 μm thick foils were used on MUR.

For MUR and TONNEAU the velocities of particles and fragments were measured and the corresponding charges identified up to Z=9 using the energy-loss versus time-of-flight technique (up to Z=3 for particles which stopped in the scintillator). The reference point in the time-of-flight distribution was provided by the transition point from ΔE to E regions in the proton and α distributions (13,5 MeV/u for 2 mm of NE 102 plastic scintillator). In TONNEAU, the polar localisation of the particle along the half-stave was determined by the difference between the times measured at both ends [15]. The resolution was ± 3°(FWHM). The ratio of light pulses

at both ends was used to check the absence of double hits [15]. As in previous experiments, the consistency of all calibrations was checked in two ways using all events obtained with a minimum bias trigger (2 particles in any detectors) : i) the spectra of Z = 1, 2, 3... particles obtained in detectors located at the same polar angle are identical ; and ii) these spectra vary regularly as a function of the polar angle. The calibration methods are described in detail in ref. [16, 17].

For the telescopes, kinetic energies and charges were derived from a ΔE-E measurement. The masses of the fragments were estimated from their charges. Since kinematic analyses rely on velocities, the Si telescopes were accurately calibrated by means of fragments with Z ranging from 1 to 10 and velocities selected by a high resolution magnetic spectrometer in a separate measurement.

Two triggers have been used. The minimum bias trigger is called a multiplicity trigger since any event where two detectors fired was recorded. The telescope trigger required a fragment in a telescope. Its purpose was to better study the peripheral events in which the projectile residue had a charge greater than 9 (identification limit of MUR and TONNEAU). We selected those events in which the heaviest fragment was detected in a telescope. In central and semi-central collisions, the charge of this fragment was found not to exceed 9 and the multiplicity trigger events did not suffer from the scintillator limitation for charge identification. Therefore, all results shown here, unless otherwise specified, have been obtained with the multiplicity trigger.

3. Selection of well characterized events

The first step in the analysis was to select the events in which sufficient information was collected. This was achieved by comparing the measured total parallel momentum to the projectile linear momentum [18]. We used the ratio $F = \sum_{i=1}^{\upsilon} Zi \; V_{//}i \; /$ (ZV) projectile, where Zi and $V_{//}i$ are the charge and parallel velocity of particle i, and υ is the multiplicity. Fig. 2 displays contour levels of the correlation between F and the measured charged products multiplicity or the total detected charge. Two hills are visible. One is located at F = 0.8 and corresponds to the average efficiency of the array. Its tails extends to values above 1 since many backward emitted products (negative $V_{//}$) are missed (see fig. 3). The other hill is located at low F values and small multiplicities. This corresponds to peripheral events in which the projectile-like fragment was emitted into a dead area or, for the most part, below 3° (the grazing angle was ~ 1°). A cut at F = 0.6 eliminates such events. The two hills are also visible in fig. 2b where the ordinate is the total measured charge. Point P is where all events would be located with a perfect

detector. Taking into account the geometrical efficiency only, the events would be located around point G. The average location below G is due to the detection threshold which decreases the detected charge without much reducing $\sum_{i=1}^{\nu_1} Z_i \, V_{//\,i}$.

The analyses described in this paper have been made with events having $F \geq 0.6$. The possible influence of this selection has been checked by using $F \geq 0.8$. The statistics for semi-peripheral and semi-central events decreased, but the results were not modified.

4. Impact parameter sorting

The next step was to sort the events as a function of the impact parameter. Actually, one uses a global variable which is sensitive to the violence of the collision, and the impact parameter value b_{exp} is estimated by attributing the most violent collisions to head-on collisions.

The choice of global variables best suited to experiments on nucleus-nucleus collisions up to ~ 100 MeV/u was discussed in ref. [18]. They were found to be the variables which make use of all detected products : the average parallel velocity Vav (which takes advantage of the detection threshold)

$$Vav = \sum_{i=1}^{\nu} \gamma_i \, Z_i \, V_i \cos\theta_i \Big/ \sum_{i}^{\nu} \gamma_i \, Z_i \qquad (1)$$

and the total transverse momentum $P_\perp = \sum_{i}^{\nu} p_{i\perp} = \sum_{i=1}^{\nu} \gamma_i \, Z_i \, V_i \sin\theta_i$ where ν is the multiplicity of the event. Z_i, V_i and θ_i are respectively the charge, velocity and polar angle of particle i, and $\gamma_i = \dfrac{1}{\sqrt{1 - V_i^2 / C^2}}$.

Let us look at the importance of selecting well characterized events. Fig. 3 is a contour plot of the multiplicity versus Vav. When well characterized events are selected (fig. 3 right), one observes Vav values ranging from ~ Vcm (central collisions) to ~ Vproj (peripheral) and the expected decrease of the multiplicity from central to peripheral collisions. The inclusion of poorly characterized events (fig. 3 left) pollute this correlation over the whole range of impact parameters.

For $P_\perp$, the perturbation is mostly located at peripheral collisions, as seen in fig. 4. The area of high $P_\perp$ values, corresponding to central collisions, is the same in figure 4 left and 4 right. The reason is that the most dissipative collisions selected by $P_\perp$ are not contaminated by other events. Indeed, when one (or several) particle(s) is (are)

missed, $P_\perp$ decreases and the event appears to be less dissipative, i.e. less central. Conversely, the shift in V_{av} can be negative as well as positive, causing the event to look more as well as less dissipative than it actually is. In the present analysis, events were sorted in $P_\perp$ bins at all incident energies in order to keep the most violent collisions as free as possible from contamination by other events. Assuming a geometrical correspondance between $P_\perp$ and the impact parameter, the cross section of each bin can be expressed as an experimentally estimated impact parameter, b_{exp} . The correlation between b_{exp} and the true impact parameter b has a FWHM of 1-2 fm [18, 25].

The distribution of $P_\perp$ is shown in fig. 5 left, both for all events and for well characterized events. The discarded events are mostly peripheral collisions with low $P_\perp$ values. This distribution provides us with information on the reaction mechanism. Indeed, one notices a continuous decrease at large $P_\perp$ values. Complete fusion of the two nuclei (full stopping of all nucleons) is the most dissipative process. When it occurs and the decay is isotropic, 2/3 of the available c.m. energy should be found in transverse energy. If some particles are emitted in the pre-equilibrium step and the remaining parts of the projectile and target undergo fusion, the transverse energy is almost the same. If (incomplete) fusion occured over a range of impact parameters of several fermis, then these events would have nearly the same large energy dissipation and a bump in the $P_\perp$ distribution would be seen at large $P_\perp$ values. Such a bump is seen in fig. 5 right, obtained from a simulation where incomplete fusion (after pre-equilibrium emission) has been forced to occur from 0 to 2.5 fm (200 mb). It is located at 2/3 of the projectile momentum, as expected. This bump does not exist in the case of reseparation of the two nuclei. The transfer of momentum decrease continuously from head-on collisions to peripheral collisions. The absence of a bump in the data (fig. 5, left panel) is an indication there is no significant cross section for complete fusion, incomplete fusion or full stopping events. The reaction mechanism evolves continuously with the impact parameter, which in turn justifies the continuous attribution of impact parameter values.

5. Source identification

5.1 Deep inelastic collisions

For each impact parameter bin, we draw Lorentz invariant cross section maps $d^2\sigma / \beta\perp d\beta\perp d(Y/Y_{proj})$, where Y is the particle rapidity and Y_{proj} the beam rapidity. At these energies, Y is very close to $\beta//$. Fig. 6 shows these maps at 67 MeV/u for five impact parameter bins for light particles (Z=1 and 2), and fig. 7 shows the maps for

IMF's (Z=3, 4, 5) and Z ≥ 6 (IMF's and remnants). These figures have been obtained with the impact parameter sorting based on $P_{\perp}$. Maps obtained with Vav look quite similar. The evolution of the rapidity distributions of particles with charges greater than 6 is shown in figure 8. For the most peripheral collisions (top panel), the rapidity is peaked around the projectile rapidity. This maximum decreases slightly with decreasing impact parameter. One may notice that this maximum never reaches the center of mass rapidity. As already seen in figure 5, this is another indication that the reaction mechanism continuously evolves with the impact parameter and that there is no significant cross section of incomplete fusion. Since the sorting based on $P_{\perp}$ does not use the rapidity values, the rapidity distributions obtained here are not affected by the sorting. This is an example of decoupling between the global variable used for impact parameter sorting and the distribution of an observable quantity. Usually, such decoupling is not complete. This is why we study an observable with two different, weakly correlated, global variables.

As in ref. [12] and according to the analysis detailed in [19], three sources contribute to the bidimensional distributions of figures 6 and 7. The fast source is attributed to the de-excitation of an excited (or primary) quasi-projectile nucleus. The heavy products (evaporation residues, evaporated fragments or fragments from a multifragmentation process) of this source have rapidities which decrease from the projectile rapidity to about 75 % of Yproj when the impact parameter decreases (fig. 8). In central collisions, few of them are as low as the c.m. rapidity (0.6 Yproj) and could be attributed to incomplete fusion. This point will be discussed in the next sub-section. Almost all events correspond to dissipative binary collisions after pre-equilibrium emission.

The pre-equilibrium source is located at mid-rapidity and contributes to the Z=1 and Z=2 maps. The study of this so-called mid-rapidity source is not the purpose of this paper, but we must take into account that, while these particles are mostly observed at mid-rapidity, they are emitted in all directions and their rapidities extend above Y_{proj} and below Y=0. In peripheral collisions, they are hardly visible on the maps, but their contribution is large in central collisions.

The slow source is the excited quasi-target in coincidence with the quasi-projectile nucleus. Its residues are not detected. The detection threshold eliminates also a large part of the light particles emitted by this slow source. Thus, of the two excited nuclei formed in a collision, the slow one is poorly detected. Conversely, all products from the quasi-projectile are above the detection threshold.

5.2 Fusion events ?

In figure 5-a, the absence of a bump at high $P_\perp$ values indicates that the fusion or full stopping cross section must be small at 67 MeV/u. At other energies, the same shape is observed and the same conclusion applies.

In order to estimate this cross section, we looked for events with a single source in the most dissipative collisions. For this quasi-symmetric system, the nucleon-nucleon rapidity ($Y_{NN} = 0.5\ Y_{proj}$) is close to the center of mass rapidity ($Y_{cm} = 0.6\ Y_{proj}$). Hence it is not possible to disentangle complete fusion (full stopping) events from incomplete fusion events after preequilibrium emission. In both cases the source of particle emission seems to be unique and its rapidity is close to Y_{cm}. Data obtained at 55 and 86 MeV/u are presented in fig. 9. Similar data were obtained at other energies. The upper row at each energy corresponds to b_{exp} estimated to be < 1 fm. Among these events, we have searched for those having a single source close to c.m.

Since $Z \geq 7$ fragments are observed only at large rapidities, the corresponding events were removed. The high and low rapidity regions of the Z=1 and Z=2 plots decreased only very slightly.

An additional selection of central (violent) collisions by another global variable was needed. We tried retaining only the higher half of the multiplicity distribution. This had a weak effect . The requirement of b_{exp} < 1 fm given by the average parallel velocity V_{av} [18], (chosen because it is almost uncorrelated with $P_\perp$), also had a very weak effect.

The transverse momentum directivity $D = \left|\left| \sum_i \vec{p_t^i} \right| / \sum_i \left| \vec{p_t^i} \right| \right|$ is low in very central collisions since there is no preferred azimuthal direction [2]. D was calculated separately for Yi > Ycm and Yi < Ycm since the detector thresholds affect only Yi< Ycm. Both D distributions have a maximum around 0.3 (similar to 0.4 in fig. 2, ref. 2) and their correlation is weak. Selecting events with both D values below 0.2 lead to a reduction in the quasi-projectile and quasi-target sources, but they are still dominant.

A better selectivity has been obtained using the ratio of the total transverse energy to the total c.m. longitudinal energy $E_\perp$ / $E_{//}$ [20]. This ratio is similar to the isotropy ratio [21]. For two sources located away from Ycm, this ratio is small. When the distribution of particles becomes more compact around Ycm, it increases. It is close to 2, on the average, in the limit of an isotropically decaying source located at Ycm. We have taken a less stringent requirement, i.e. $E_\perp / E_{//} > 1.5$. One then obtains the lower row at each energy in fig. 9 where the quasi-projectile and quasi-target sources are

strongly reduced, especially at the lower incident energies - most events in the lower rows arise from a different mechanism than the main portion in the upper rows.

Since events in both rows have the same measured total parallel momentum and total charge distributions, these events cannot simply be less well characterized events just satisfying by chance the selection criteria. There are some such possible fusion events at b_{exp} values up to 3 fm. By relaxing the selection criteria, one gets an *upper limit* for the fusion cross section of 30 mb at 55 MeV/u. This limit is lower at higher energies. This can be compared to the geometrical overlap cross section which is < 30 mb, since full overlap occurs below 1 fm for this nearly symmetric system.

A thorough study of the question of binary reactions versus incomplete fusion in central collisions requires a comparison of the data to several dynamical calculations filtered by the response of the experimental set-up. Such a study has been made for the present data and for data obtained in $^{64}Zn+^{nat}Ti$ collisions from 35 to 79 MeV/u [25]. In these nearly symmetric systems, the fusion cross section reaches 150 mb at 35 MeV/u and is lower than 20 mb at energies above 50 MeV/u.

We conclude that at all impact parameters the collisions lead to the formation of two main primary products accompanied by a "mid-rapidity" emission of light particles. As we will see in the next sections, the mass of the quasi-projectile source is lower or close to the projectile mass and the relative velocity of the fragments is strongly reduced. This reaction mechanism is very close to deep inelastic collisions known at lower energies, but there are two differences : i) for light systems at low energies, deep inelastic process occurs only in semi-peripheral reactions, whereas here the whole range of impact parameters is concerned ; and ii) the quasi-projectile and quasi-target are accompanied by preequilibrium emission. It is also close to the participant-spectator model (valid at higher energies), but here the excitation energies of the two "spectators" contain a large part of the available energy, as we will see in section 6.3. Actually, a continuous evolution of the reaction mechanism occurs from low to high energies.

The few possible fusion events have been removed and the analysis was continued with the remaining events. The inclusion or exclusion of these events had, in fact, a negligible effect on the results shown hereafter.

6. Characteristics of the quasi-projectile

Since all products from the quasi-projectile are well above the detection threshold and their charges are well identified, we can determine the velocity, mass (or charge)

and excitation energy of the primary excited quasi-projectile nucleus left after pre-equilibrium emission.

In ref. 12, the source velocity in each b_{exp} bin was taken as the centroid of the parallel velocity distribution of the detected heavy residues (Z>6). Here the source velocity vector was reconstructed for each event from the momentum vectors of its products with $Z \geq 2$. Z=1 particles were excluded since the rapidity distributions from the "mid-rapidity" and quasi-projectile sources overlapped very much with each other. For Z=2, a cut on Y around Ycm eliminated a fraction of the "mid-rapidity" particles and retained most of the products from the primary nucleus. A variation of ± 10 % on the value of this operational cut was found to have negligible effect on the results. Almost all $Z \geq 3$ products were emitted from the quasi-projectile.

In order to quantify the relative motion damping seen in fig. 6 and 7, the velocity (or kinetic energy per nucleon) and deflection angle of the quasi-projectile source can be plotted in the center-of-mass. The distribution obtained with all well characterized events is shown in fig. 10 top left at 55 MeV/u. The grazing angle is ~1° and one observes a broad range of energy damping and deflection angle (called bounce-off angle at relativistic energies [37]). This distribution is deformed for several causes : i) the minimum detection angle of 3.2° excludes the detection of peripheral collisions at small angles ; ii) the small proportion of well characterized semi-peripheral collisions (fig. 5) strongly reduces the number of events at energies close to elastic scattering ; and iii) all experimental widths and losses of resolution on velocities and angles contribute to broadening the distributions along both directions. Very few events have a kinetic energy close to full damping of the relative motion. A more quantitative view is shown in the right panel, where the mean kinetic energy and mean deflection angle are plotted for each b_{exp} bin. The point labelled 1.5 corresponds to $b_{exp} < 1.5$ fm, the point labelled 2.5 corresponds to b_{exp} = 1.5 to 2.5 fm, and so on. The increase of energy damping and deflection angle from peripheral to central collisions characterizes deep inelastic collisions. At 95 MeV/u (bottom panels), the same evolution is observed. There complete damping of the relative motion is no longer visible. This confirms that the fusion or full stopping cross section must be very small. The evolution observed is that of a binary dissipative process (deep inelastic collisions) where the strongest energy damping and the largest deflection angles belong to central collisions. The right-hand vertical scale shows the corresponding dissipated energy per nucleon. The right-hand and left-hand scales are not identical (with opposite directions) since the system is not symmetric.

One can now plot the distribution of particles versus their velocity components parallel and perpendicular to the direction of the reconstructed quasi-projectile. Such

distributions in the rest frame of the quasi-projectile are shown in fig. 11 at the lowest incident energy (55 MeV/u) and in fig. 12 at the highest energy (95 MeV/u) for central and semi-peripheral collisions. They are quite similar. The nearly isotropic emission from hot nuclei is seen for all fragments. The pre-equilibrium and quasi-target components are seen for light products, mostly at negative $\beta_{//}$ values.

6.1 Angular distributions

We now turn to the question of ascertaining if the quasi-projectile was in thermal equilibrium. To begin with, the memory of the initial direction of the projectile must have been lost in the direction of all the products emitted in the rest frame of the quasi-projectile, except for the angular momentum brought in by the projectile. A global indication is given by the value of the isotropy ratio [21]. As in fig. 3 of ref. [12], it is close to 1 at all energies and impact parameters. A more sensitive test is given by the polar angular distribution of each product in the frame of the quasi-projectile. It must be isotropic in the absence of angular momentum and evolve towards $1 / \sin \theta$ as the angular momentum increases. The angular distributions of Z=2 particles (mostly α-particles) are displayed in fig. 13 for several impact parameter bins. The 3.2° hole in the MUR is responsible for the decrease near 0°. This decrease extends well beyond 3.2° as the hole has a much larger opening angle in the frame of the quasi-projectile and because the quasi-projectile is not moving along the beam axis. Above 90° the contribution of the two other sources gradually increases. Below 90° the distribution is flat for central collisions and gradually evolves towards a $1/\sin \theta$ distribution as the angular momentum of the quasi-projectile increases with increasing impact parameter. For Z=3-5 clusters, the results are quite similar : fig. 14. For Z=1 particles (mostly protons), the anisotropy is less marked, as expected for lighter particles. This shape of the angular distribution below 90° is consistent with emission from an equilibrated nucleus.

6.2. Masses of residual and primary quasi-projectiles

The average mass of the heaviest fragment from the quasi-projectile, detected in a telescope, is shown in fig. 15 as a function of the experimentally determined impact parameter, for the five incident energies. At each energy, this average residual mass decreases from peripheral to central collisions. This variation is consistent with a larger energy dissipation in central collisions, whatever the energy deposition and de-excitation processes are. The distribution shifts to lower values of Z when the incident energy increases, indicating an increase in the deposited energy. At 95 MeV, the average mass of this heaviest fragment is less than 12. Detailed distributions are presented in fig. 18 and will be discussed later.

The quasi-projectile mass can be reconstructed by adding up the masses of the detected products and taking into account the geometrical efficiency. Three difficulties occur however. Firstly, only the charge of the fragment is measured. Since the initial system has almost the same numbers of neutrons and protons and de-excitation favours the formation of residues along the β stability line, we take the mass of $Z \geq 3$ products as 2 * Z. For Z=1 and Z=2 additionnal NaI detectors provided us with the proportion of p, d and t for Z=1 (mostly p, ~ 30 % d, 5 % t) and Z=2 (more than 90 % are α-particles). These proportions vary slightly with E_{inc} and b_{exp}. Secondly, pre-equilibrium particles contribute to the mass. As in ref. [12], the best way of minimizing this contribution is to take for each event the products emitted in the forward hemisphere in the rest frame of the quasi-projectile (fast source, see fig. 10-11) and multiply their contributions by 2 in order to get the emission over 4 π. Actually, in order to avoid meaningless fluctuations of the reconstructed mass, especially in peripheral collisions, the mass of the heaviest fragment was included, whatever hemisphere it was in. The mass of other products in the forward hemisphere was multiplied by 2 and added to the mass of the heaviest fragment. One must keep in mind that some pre-equilibrium contribution remains and the reconstructed mass is an upper limit of the quasi-projectile mass, especially in central collisions. Thirdly, neutrons are not detected. We attributed to each event the number of neutrons which is necessary to arrive at the charge-to-mass ratio of the initial system.

This method leads to large fluctuations event-by-event, but the mean value in each b_{exp} bin is correct. The mean mass of this quasi-projectile remains below the projectile mass at all impact parameters, in agreement with the binary character of the collision. This low value excludes a massive transfer process where mass is transferred from the light initial partner (here the target) to the heavy one (here the projectile). The increase seen in very central collisions is due to the contribution of pre-equilibrium particles. Simulations with a code including pre-equilibrium emission from the interaction zone (QMD [22] or Landau-Vlasov [24]) have shown that this contribution can reach 10% in the most central collisions at 95 MeV/u.

A comparison to a Landau-Vlasov code [24] using a momentum dependent Gogny D1-G1 force is shown in figure 15 . The mid-rapidity source is observed to be stronger than in the experiment. The closed triangles show the mass of the fast source when it separates from the target-like source, after a time of around 70-90 fm/c, depending on b. At 6 fm, it is equal to the experimentally reconstructed mass but is lower at 2 fm. Experimentally, the mass at separation cannot be determined beyond the fact it is intermediate between the reconstructed mass and the residual mass. The calculated angular distribution of emitted particles after separation is isotropic in the quasi-projectile source frame. Part of the emission prior to separation is also isotropic in this frame. Therefore, the mass of the isotropically decaying calculated source is close

to the experimentally reconstructed mass [13]. Closed circles show the calculated residual masses at a large time (800 fm/c), in good agreement with the measured masses.

6.3 Excitation energies per nucleon

In order to obtain the excitation energy of the quasi-projectile, calorimetry can be used whereby one sums the kinetic energies of all its products in its reference frame and takes into account the mass balance. The same difficulties as for determining the primary mass occur. The average kinetic energy of neutrons is taken to be that of protons in the same bin. Again, only particles emitted in the forward 2π of the quasi-projectile are taken and their contribution is multiplied by 2 [12].

Since the quasi-projectile mass varies with impact parameter and incident energy, it is more meaningful to look at the excitation energy per nucleon. Its average value in each b_{exp} bin is shown in fig. 16. As expected, it increases from peripheral to central collisions and with the incident energy. In semi-peripheral collisions, the values obtained correspond to upper values rather than to average values. Indeed, the grazing angle is ~1° and, in order to get a well characterized event, the projectile-like residue must have been emitted above 3°. This is less probable for nuclei with low excitation energy which emit fewer and slower particles than hotter nuclei. In central collisions, the values obtained at 55 and 67 MeV/u are larger than the values obtained at 55 and 65 MeV/u in ref. [12]. This is the consequence of the modifications described earlier: i) use of ^{36}Ar instead of ^{40}Ar (less neutrons are emitted at high temperature and more excitation energy is available for charged particles), ii) impact parameter sorting based on $P_{\perp}$ which prevents high excitation events from being contaminated by lower excitation events (discussed in section 4) and iii) the transverse component of the quasi-projectile velocity is determined for each event in addition to the component along the beam axis.

Such results are sensitive to the completeness of the measurement. The high efficiency of detection made it possible to sort the events as a function of the violence of the collision. The detection of the charged products of the fast primary nucleus was limited only by the geometrical efficiency (~ 85 %) since all its products had velocities above the thresholds. The cross section of events in the first bin is 70 mb (b_{exp} = 0 to 1.5 fm). If, for instance, 500 mb of "central" collisions were analyzed together (that is b_{exp} from 0 to 4 fm), < E*/A> would reach only ~ 7 and 8 MeV/nucleon at 55 and 95 MeV/u, respectively, instead of 8 and 11 MeV. The small difference between 7 and 8 would look like a tendency to saturation.

As noted in the previous section, some pre-equilibrium light particles are included in the reconstructed quasi-projectile mass and contribute to its excitation energy. At most this contribution is 15%.

At 55 and 95 MeV/u, these mean excitation energies per nucleon are close to the mean dissipated energies per nucleon in the same b_{exp} bin (fig. 10). Since the mass of the quasi-projectile is lower than the projectile mass, the total excitation energy is lower than the total dissipated energy, the difference being given to pre-equilibrium emission.

7. Decay of the quasi-projectile

We can now study the de-excitation of these excited quasi-projectiles. The results relative to the multiplicities of various products and the mass distributions as a function of the excitation energy per nucleon will be shown first, then the kinetic energy distributions will be studied. They are compared to calculations assuming sequential statistical decay. We did not study the process which leads to the formation of the excited primary nuclei ; we assumed only that nuclei with masses of ~36 have been formed at excitation energies up to 11 MeV/nucleon and we have investigated at their decay. Sequential statistical decay (evaporation) was used with the Transition State Model in the code EUGENE [23]. The de-excitation of excited emitted fragments was followed until they can no longer emit nucleons. In this approach a parameter controls the influence of the potential energy barriers on the binary partitions on the decay widths, but does not effect the final fragments energy spectra, so we have simply chosen the barriers at the conditional saddle. Instead, three parameterizations of the level density parameter have been used : $E^* = a\ T^2$ with a = A/8 and A/13, respectively, and the level density according to ref. [27]. It should be noted that, with this comparison, we are not aiming at a full description of the data by adjusting the input parameters of the simulation, but we wish to demonstrate the limitation of sequential binary decay model.

7.1. Multiplicities of products

As above the products considered are those emitted in the forward 2π of the primary nucleus source, multiplied by 2 and corrected for the geometrical acceptance of the set-up. Fig. 17 shows the multiplicities of Z=1, Z=2 and other products as a function of the excitation energy per nucleon. There is no dependence on the incident energy. The multiplicity for Z=1 increases linearly with E*/A, whereas the multiplicity for Z=2 increases linearly up to ~ 4 MeV/nucleon, after which the disassembly becomes more complete. The multiplicity for $Z \geq 3$ increases with the excitation energy, but it

saturates and tends to decrease at high excitation energies since more light charged particles are emitted. At a fixed excitation energy, the mass decrease of the primary nucleus with the incident energy leads to a decrease of this mulitplicity with excitation energy. The lines are the results of calculations.

A/8 and A/13 give a good fit of the total multiplicity increase with E*/A but no prescription reproduces the behavior of specific products. While too many Z = 1 particles are predicted to be emitted, the multiplicities for Z = 2 and heavier fragments are underestimated. This is an indication that sequential decay of a thermal source cannot explain the data.

7.2 Charge distributions

As already indicated by fig. 17, the mass distributions of products from the quasi-projectile are the same for the same excitation energy obtained at different sets of incident energy and impact parameter. This is shown in fig. 18 for three excitation energy bins : 2.5-3.5, 5.3-6.1 and > 9.5 MeV/u (corrected values). One observes a strong variation with the excitation energy. At 3 MeV/u a peak due to evaporation residues is located at Z=10-14. This peak shifts to lower Z values and almost disappears at ~6 MeV/u. IMF's, already present at 3 MeV/u, dominate above 6 MeV/u. The evolution towards lighter products continues up to 9.5 MeV/u where the multipicity for Z > 8 is very small.

As in figure 15, at a fixed incident energy, the variation of the mass distribution with the excitation energy is linked to a variation in the impact parameter : a heavy residue is still seen in semi-peripheral collisions while IMF's dominate in central collisions.

7.3. Shape of kinetic energy distributions

If the particles are emitted by a thermal source, one can use their kinetic distributions in the emitter frame to extract information on the temperature of the primary nucleus. In order to minimize the pre-equilibrium contribution, these spectra have to be taken at forward angles in the frame of the primary nucleus.

These spectra were fitted with the function,

$$W(E) = \alpha \frac{(E - B)}{S^2} \exp\left(-\frac{(E - B)}{S}\right) \qquad (2)$$

where S is the slope parameter, B a barrier parameter and α a normalization constant.

In the forward 2π in the rest frame of the quasi-projectile, the stability of S is seen in fig. 19, where spectra were constructed from 20° to 80°. The value of S fluctuates

from 9.7 to 10.3 ± 0.4 MeV. The same stability was found at all energies and impact parameters.

Fig. 20 shows an example of fits at the highest incident energy, 95 MeV/u. It displays the kinetic energy distributions for Z = 2 particles (mostly α-particles) emitted by the fast primary nucleus in the interval 35°-60°. The residual part seen at high energies is due to pre-equilibrium emission. Fits made by hand of the high energy part of the spectra would lead to higher values of S in central and semi-central collisions. That means the S values obtained with formula (2) are the lowest values which can be obtained.

The whole set of S values obtained for Z=2 particles is displayed in fig. 21. The behavior is quite similar to that for E*/A (fig. 16) - an increase with incident energy and from peripheral to central collisions. Here also, one sees the importance of a rather complete detection of events.

These slope parameters are equal to the apparent temperature (average temperature along the de-excitation chain) only if all the excitation energy is thermal. According to statistical de-excitation calculations, these apparent temperatures would correspond to initial temperatures of 9-10 MeV (fig. 9 in ref. 12).

Actually, spectra such as those of fig. 19 and 20 are basically incorrect [7], the reason being that one should take into account cumulative recoil effects due to the successive emission of particles and plot for each particle its real kinetic energy. This would require , for each event, knowledge of the order of emission of the detected particles (and also undetected neutrons). Since we do not have such information the kinetic energy is obtained in the reference frame of the primary nucleus. This is correct only for the first (unknown) emitted particle in each event. This effect distorts the shape of the spectrum and makes it impossible to use the absolute values of S as measures of the apparent temperatures. Simulations show that this distortion is a broadening of the kinetic energy distribution, which increases the value of S. This broadening is seen also in the low energy part of the spectrum and leads to zero or negative values of the barrier B. The relative variation of S with b_{exp} or E^*/A is merely a qualitative piece of information, not a quantitative one. This is true especially for the light nuclei studied here, as well as for heavy nuclei when they emit IMF's or many particles.

8. Summary and conclusions

The charged products (light particles and fragments) emitted in the interaction of ^{36}Ar on ^{27}Al have been detected at energies ranging from 55 to 95 MeV/u. Their charge and velocities were measured. Well characterized events have been selected in

the analysis, thereby eliminating mostly peripheral events. These well characterized events have been sorted as a function of the violence of the collision via the sum of transverse momentum, which avoids the most violent collisions from being contaminated by less violent collisions. Expressed as impact parameter values, this sorting allowed us to study events between 0 and 75% of the grazing impact parameter.

In very central collisions, a very small cross section (< 1% of the reaction cross section) can be attributed to single (c.m.) source events. At lower incident energies such events are simply complete fusion events. Here they are likely due to incomplete fusion, i.e. pre-equilibrium emission followed by fusion of the remaining parts of the projectile and target. At energies above 250 MeV/u, in "full stopping" events all nucleons are issued from the mid-rapidity source. Such events have been observed for the neighbouring system Ca+Ca [26]. In complete fusion, incomplete fusion after pre-equilibrium emission or full stopping, the whole available c.m. energy is transformed into other degrees of freedom. The evolution of reaction mechanisms with energy for these most dissipative collisions is indicated by the long dashed line in fig. 22.

Apart this small cross section, at the energies studied here, two main primary products, a quasi-projectile and a quasi-target (products of deep inelastic collisions, or "spectators"), are formed after pre-equilibrium emission (mid-rapidity source, participants) at all impact parameters. The reaction mechanism evolves continuously from deep inelastic collisions at low incident energies to a participant-spectator process at higher beam energies. Two characteristics evolve with the beam energy : i) the range of impact parameter increases from semi-peripheral reactions at low energies to semi-central and central collisions at energies above the Fermi energy ; ii) the number of particles emitted from the interaction zone in the first step of the collision becomes noticeable around the Fermi energy and becomes a large part of the system at relativistic energies.

In figure 22 is schematized the evolution of reaction mechanims with energy for central collisions below ~4% of σ_R (b_{exp}<1.5 fm). The solid line represents the proportion of the available energy transformed from relative motion into other degrees of freedom (Total Kinetic Energy Loss TKEL, dissipated energy). The short dashed line is the part given as excitation energy to the mono or di-nuclear system. The TKEL and excitation energy at 55 and 95 MeV/u have been estimated from the mean kinetic energy (fig. 10), mean mass (fig. 15, corrected for the pre-equilibrium contribution) and mean excitation energy (fig. 16) of the quasi-projectile in the 70 mb of most violent collisions. At low energies, fusion occurs at these impact parameters. When deep inelastic collisions replace fusion, the relative motion is fully damped, i.e. the kinetic energy of the quasi-projectile and quasi-target is equal to their Coulomb repulsion, and their total excitation energy is close to the available energy. At the beam energies

studied here, the dissipated energy and the excitation energy are lower fractions of the available energy. Note that the plotted values are mean values in the 70 mb bin. It contains very violent events with a larger damping of the relative motion (left panels in fig. 10) and larger values of excitation energy. At high beam energies, the quasi-projectile and quasi-target have a low excitation energy per nucleon and a small mass [28, 29] and the name of spectators is justified. Above 100 MeV/u, the TKEL line might decrease less than indicated, since the remaining relative motion of the spectators depend on two opposite trends when the beam energy increases: the energy per nucleon of the spectator remains a larger part of the initial relative motion, but its mass decreases (the extreme situation is one nucleon with the beam velocity).

The dotted line shows the part of available energy carried by emission from the interaction zone. It is the difference between the TKEL and excitation energy. Therefore it is subject to a very large error and should be taken as indicative. Around the Fermi energy, pre-equilibrium emission sets in and becomes more important with the beam energy. At several hundreds of MeV/u, the participants carry most of the dissipated energy.

Since all products from the quasi-projectile were detected with a high efficiency, the characteristics of the primary quasi-projectile could be determined event-by-event. Its reconstructed mass was found to be slightly lower than the projectile mass and was found to decrease with increasing incident energy and from peripheral to central collisions. The mass of the heaviest was found to decrease with decreasing impact parameter, and to decrease slightly with the increasing incident energy.

The excitation energy was obtained from the kinetic energies of the detected products and the mass balance. It increases with increasing incident energy and decreasing impact parameter. In the 70 mb of most violent collisions (b_{exp} from 0 to 1.5 fm), average excitation energies above 10 MeV per nucleon were reached. Half of the available c.m. energy per nucleon is transformed from relative motion into excitation in central collisions.

The present data show that the production of hot spectator does not require the use of very heavy projectiles and very high energies. With Au projectile at 600 MeV/u, <E*/A> values and mean spectator masses of ~8 MeV and ~30 nucleons were obtained in ref. 28 ; these values rise to ~15 MeV and ~55 nucleons in ref. 29. In the present work, < E*/A> above 11 MeV and masses ~35 nucleons were obtained with Ar projectiles at 95 MeV/u on 70 mb and a more detailed sorting would lead to larger <E*/A> values on a smaller cross section.

In central collisions, the products from the quasi-projectile were emitted isotropically in its rest frame, indicating that thermal equilibrium could have been reached. When the impact parameter increases, transferred orbital angular momenta leads to favoured emission along the direction of the quasi-projectile.

The high energy slope parameters of the kinetic energy distributions were observed to increase from peripheral to central collisions and with the incident energy. In central collisions, values of 12 MeV were obtained. Due to the emission of a large part of the primary mass, these slope parameter values are merely upper limits of the apparent temperatures.

When studying the mass distributions and the kinetic energy distributions as a function of the product charge, the dominant parameter was found to be the excitation energy.

Sequential statistical emission of products could not explain the mass distributions. The same conclusions were obtained in the analysis of 64Zn on Ti collisions from 35 to 79 MeV/u, with the same experimental set-up and methods [19, 25]. Very recently similar conclusions were reached on Ar+KCl (35 to 74 MeV/u) and Xe+Sn (25 to 50 MeV/u) studied with the 4π array Indra in events where the quasi-target was also reconstructed [30].

REFERENCES

[1] E. Suraud et al ; Progress of Nuclear and Particle Sciences 23 (1989) 357

[2] J.P. Alard et al ; Phys. Rev. Lett. 69 (1992) 889

[3] O. Granier et al ; Phys. Lett. B309 (1993) 10

[4] B. Lott et al ; Phys. Rev. Lett. 68 (1992) 3141

[5] B.M. Quednau et al ; Phys. Lett. B309 (1993) 10

[6] M.F. Rivet et al ; Proc. XXXI Int. Winter Meeting on Nuclear Physics, Bormio (Italy), 1993

[7] E. Vient et al ; Nuc. Phys. A571 (1994) 588

[8] E. Plagnol et al ; Phys. Lett. B221 (1989) 11

[9] G. Auger et al ; Phys. Lett. B169 (1986) 161

[10] R. Dayras et al ; Nucl. Phys. A460 (1986) 299-323

[11] L.G. Moretto, G.J. Wozniak ; Ann. Rev. Nuc. Sci. (1993) p. 379-455, and references therein.

[12] D. Cussol et al ; Nucl. Phys. A561 (1993) 298

[13] P. Eudes ; in preparation

[14] G. Bizard et al ; Nucl. and Inst. Meth. A244 (1986) 489

[15] A. Péghaire et al ; Nucl. and Inst. Meth. A295 (1990) 365

[16] J.C. Angélique ; Ph D thesis, Université de Caen (1993)

[17] A. Kérambrun ; Ph D thesis, Université de Caen (1993)

[18] J. Péter et al ; Nucl. Phys. A 519 (1990) 611

[19] A. Kérambrun et al ; report LPC Caen 94-14 and in preparation

[20] S.C. Jeong et al ; Proc. XXX Winter Meeting on Nuclear Physics, Bormio (1992), GSI preprint 93-38
W. Reisdorf et al ; Proc. Int. Workshop on Nuclear Excitations XX, Hirschegg (1992)

[21] H. Ströbele et al ; Phys. Rev. C27 (1983) 1349

[22] J. Aichelin and H. Stöcker ; Phys. Lett. B176 (1986) 14

[23] D. Durand ; Nucl. Phys. A541 (1992) 266

[24] B. Remaud et al ; Nucl. Phys. A447 (1985) 555c

[25] J.C. Steckmeyer et al , talk at XXXII Int. Winter Meeting on Nuclear Physics, Bormio (Italy), 1995

[26] H.H. Gutbrod, K.H. Kampert, B.W. Kolb, A.M. Poskanzer, H.G. Ritter, H.R. Schmidt ; prepring GSI 90-07

[27] C. Guet et al ; Phys. Lett. B205 (1988) 427

[28] A.S. Botvina et al ; Nucl. Phys. A584 (1995) 737

[29] J.. Pochodzalla et al ; preprint GSI 95-13

[30] V. Métivier et al ; Communication at XXXII Int. Winter Meeting on Nuclear Physics, Bormio (Italy), 1995

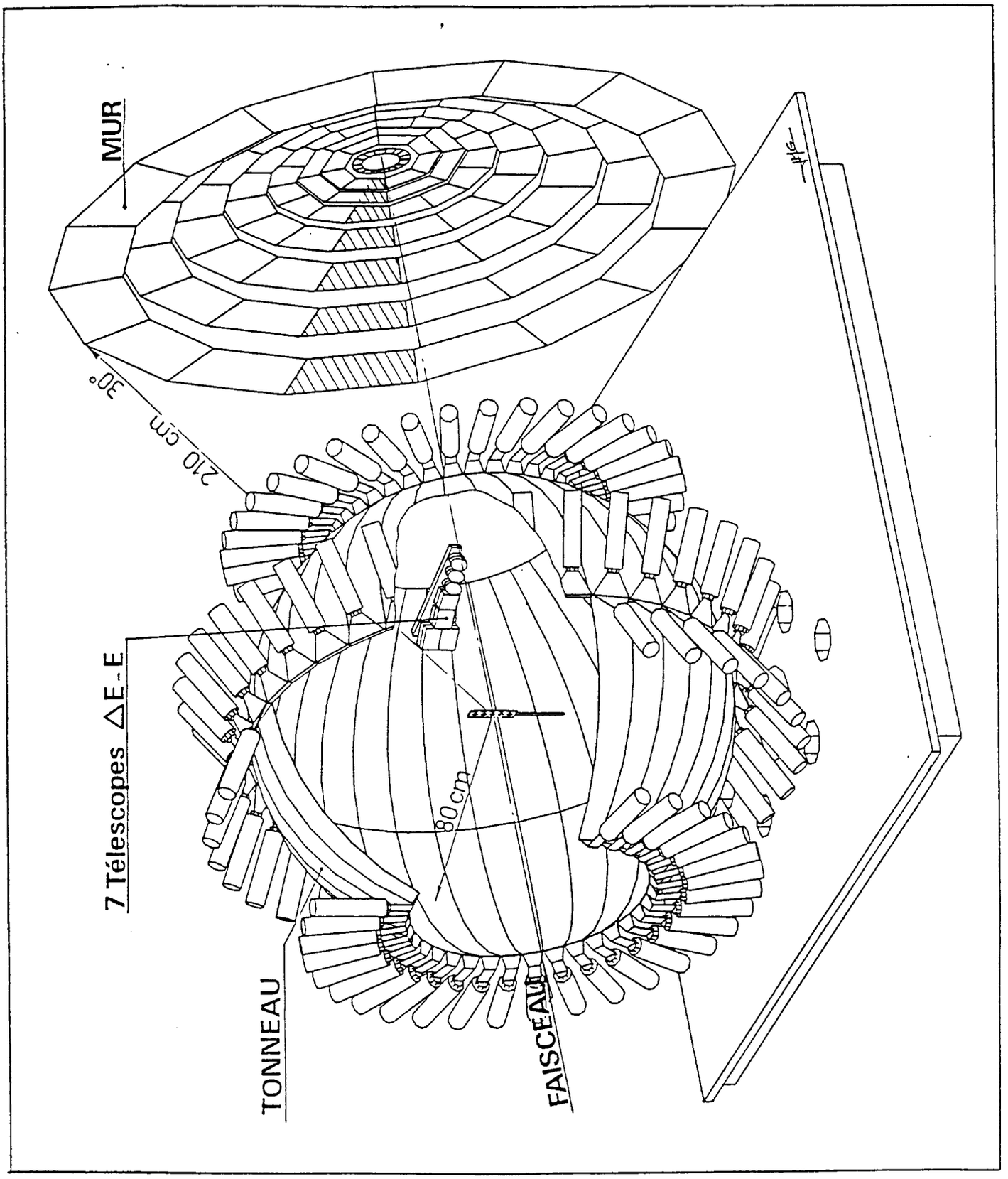

1 - Experimental set up

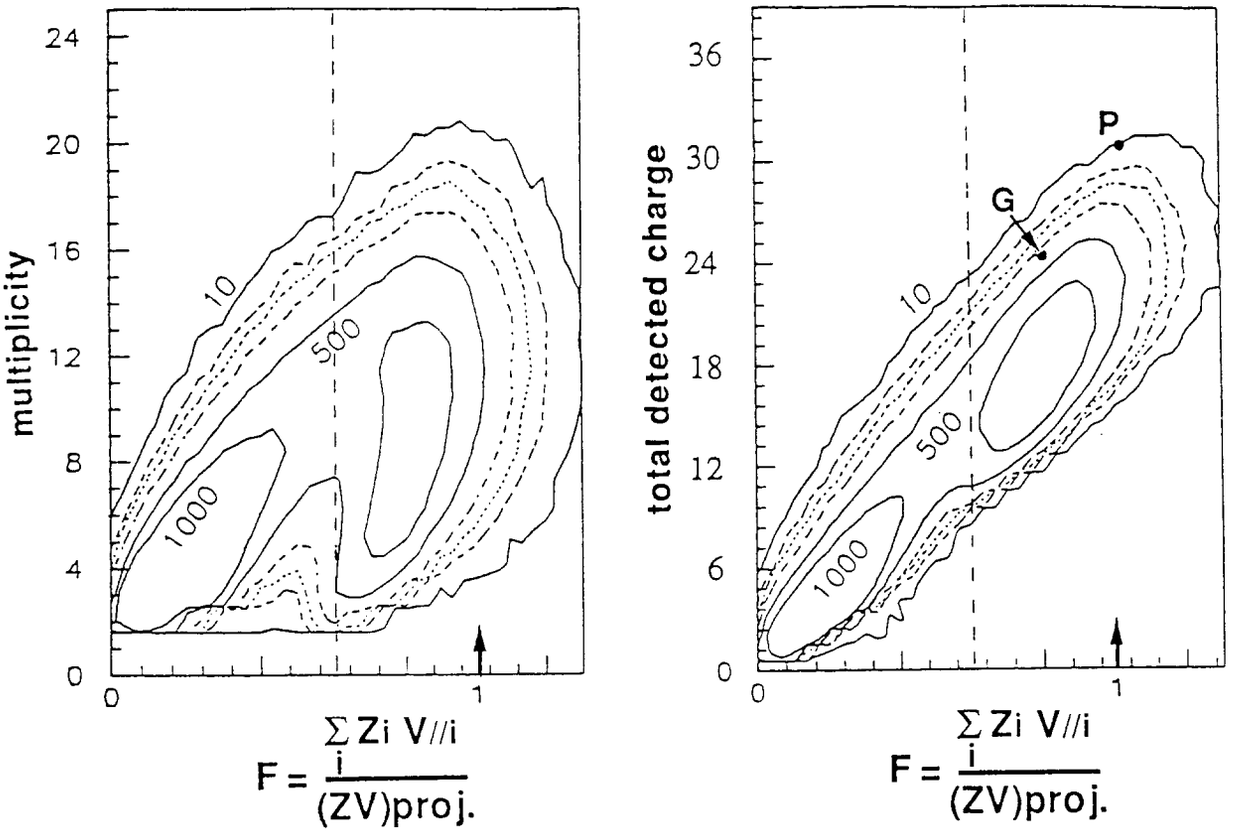

2 - Selection of well characterized events at 67 MeV/u . *Left* : logarithmic contour plot of the measured multiplicity versus the measured proportion of the projectile charge linear momentum, F . *Right* : logarithmic contour plot of the total detected charge versus F . With a perfect detector all events should be at P . G is the center of the area reached in taking into account the average geometrical efficiency. The hill below G is due to the velocity threshold and the hill at very low total charge and F values is due to the opening for the beam (see text).

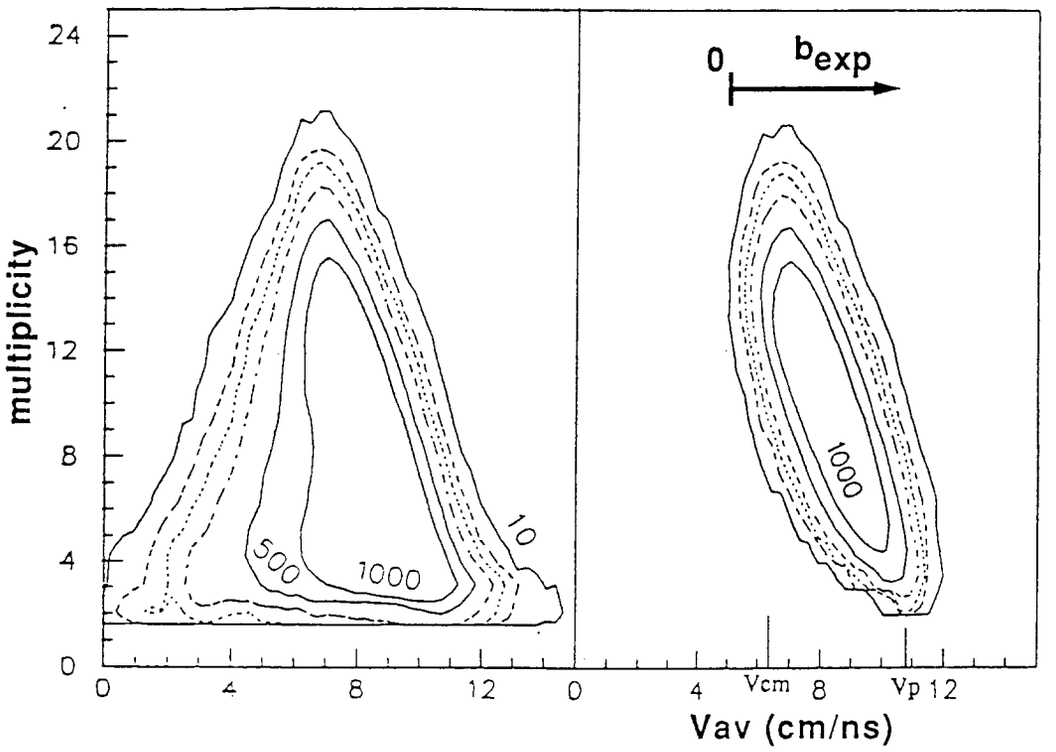

3 - Impact parameter sorting with the average (mass weighted) parallel velocity V_{av} at 67 MeV/u . *Left* : logarithmic contour plot of the multipicity versus V_{av} for all detected events. *Right* : same figure after selection of well characterized events (F>0.6, see fig. 2).

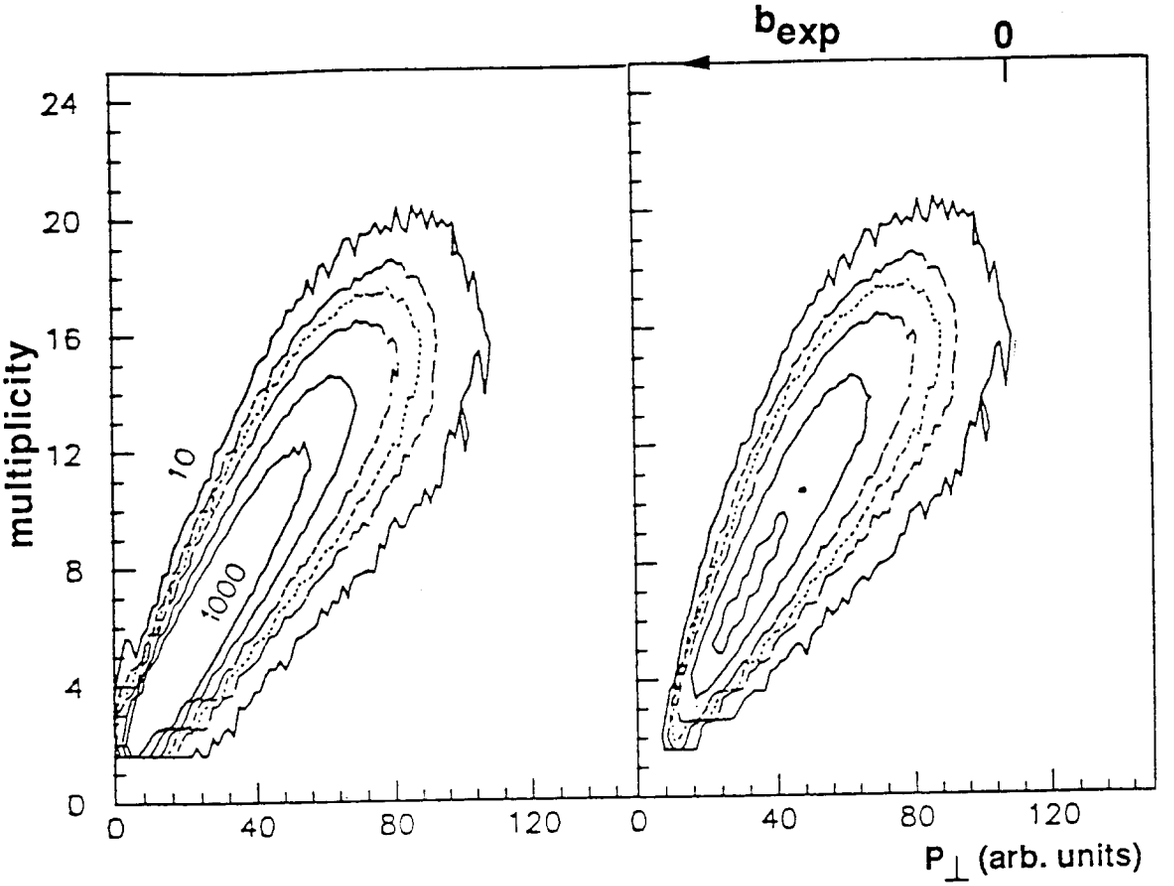

4 - Same as fig.3, but with the sum of transverse momenta $P_\perp$ as abcissa.

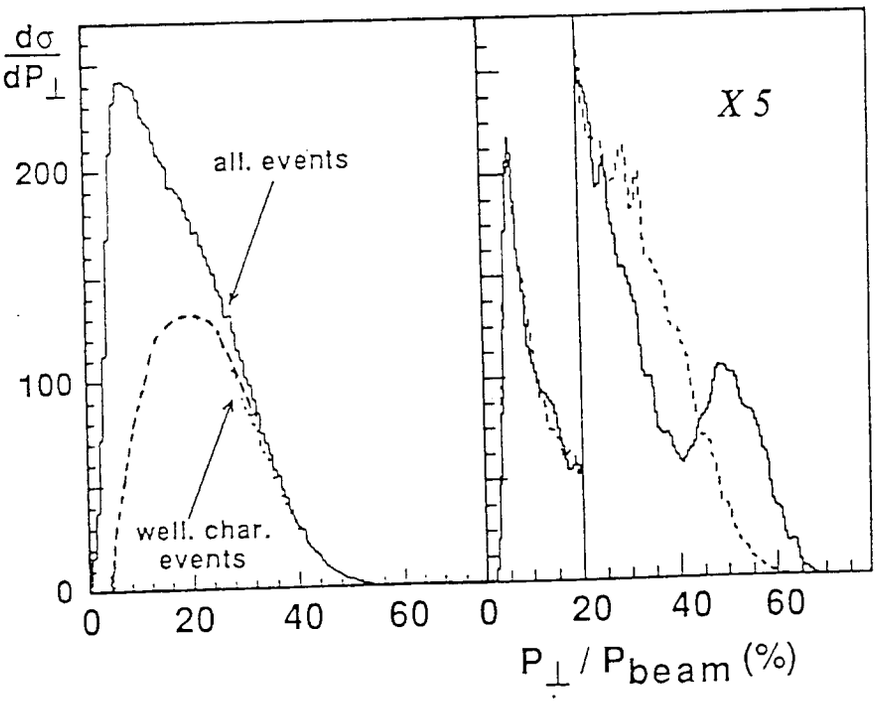

5 - Distribution of the sum of transverse momenta, $P_\perp$, at 67 MeV/u. *Left* : experimental data. Solid line : all detected events. Dashed line : well characterized events. *Right* : simulation. Solid line : assuming an incomplete fusion cross section of 200 mb (i.e. from b=0 to b=2.5 fm). Dashed line : assuming a binary reaction mechanism over the wole range of impact parameter.

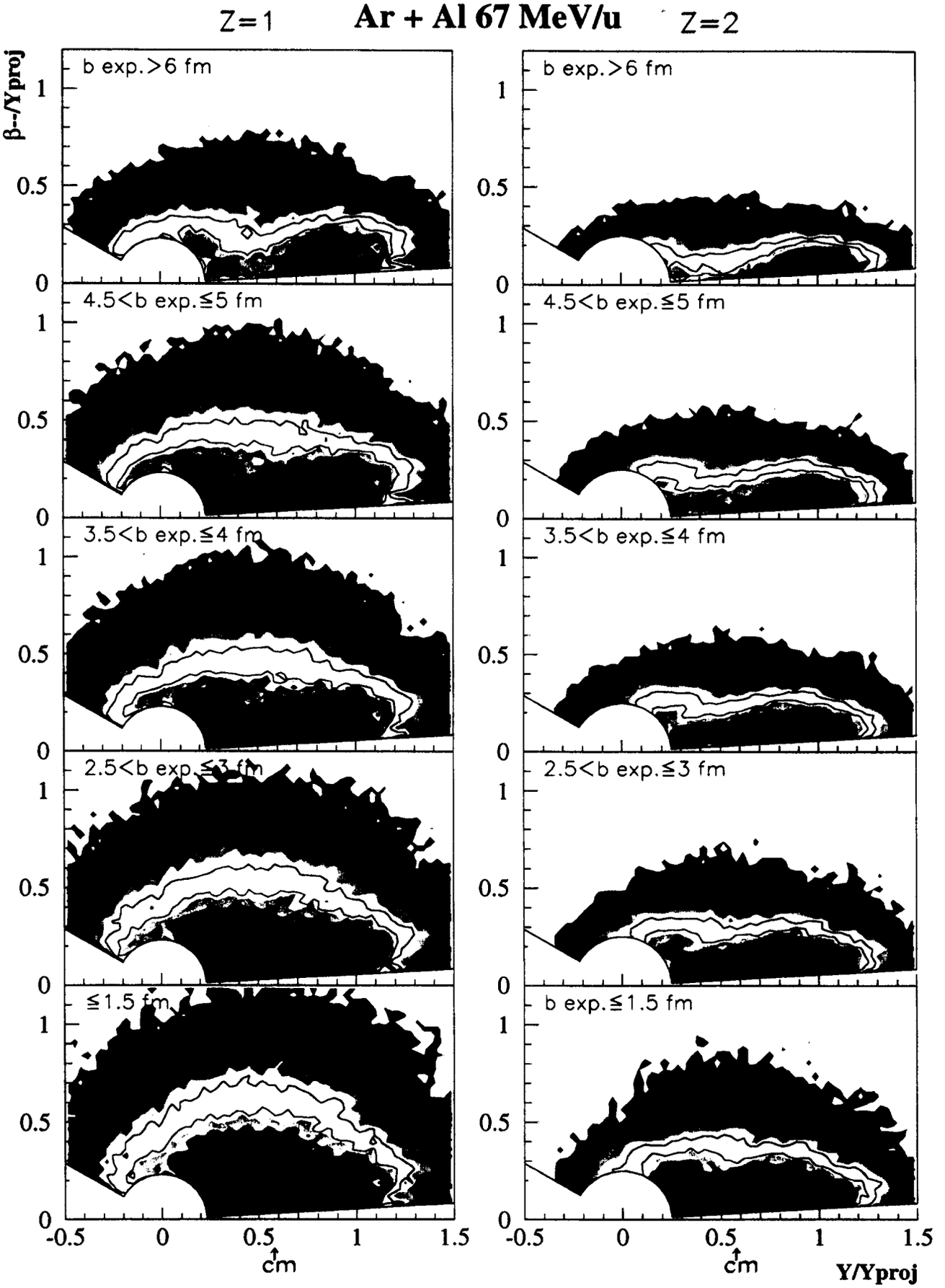

6 - Logarithmic Lorentz invariant cross sections (arbitrary units) in the laboratory. The transverse rapidity (β_+) and the rapidity are both normalized to the projectile rapidity. *From top to bottom* : from peripheral to central collisions. *Left* : Z=1 particles (mostly protons). *Right* : Z=2 particles (mostly α-particles).

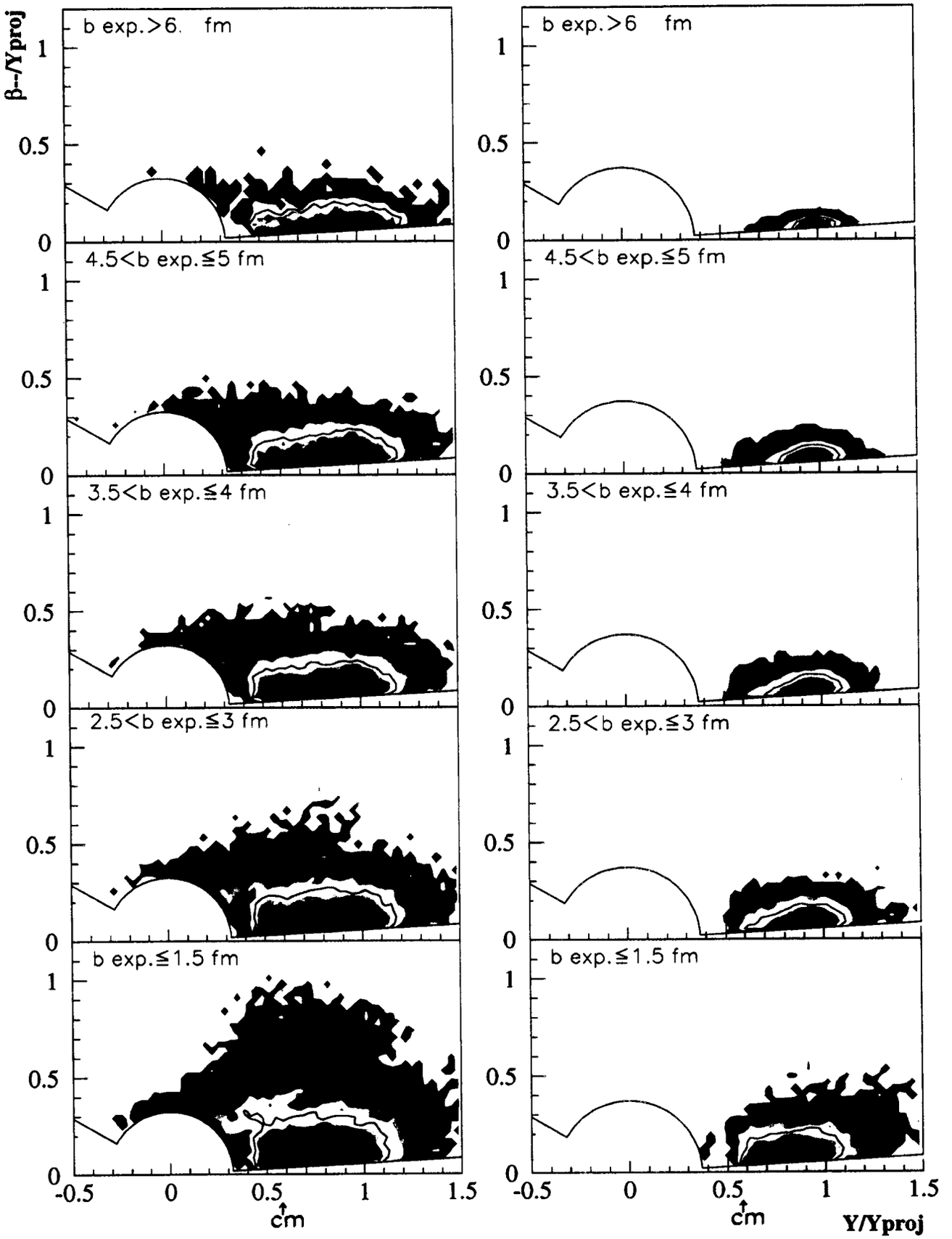

7 - Same as fig. 3 for IMF's (Z=3, 4, 5) and for heavy fragments (Z≥6).

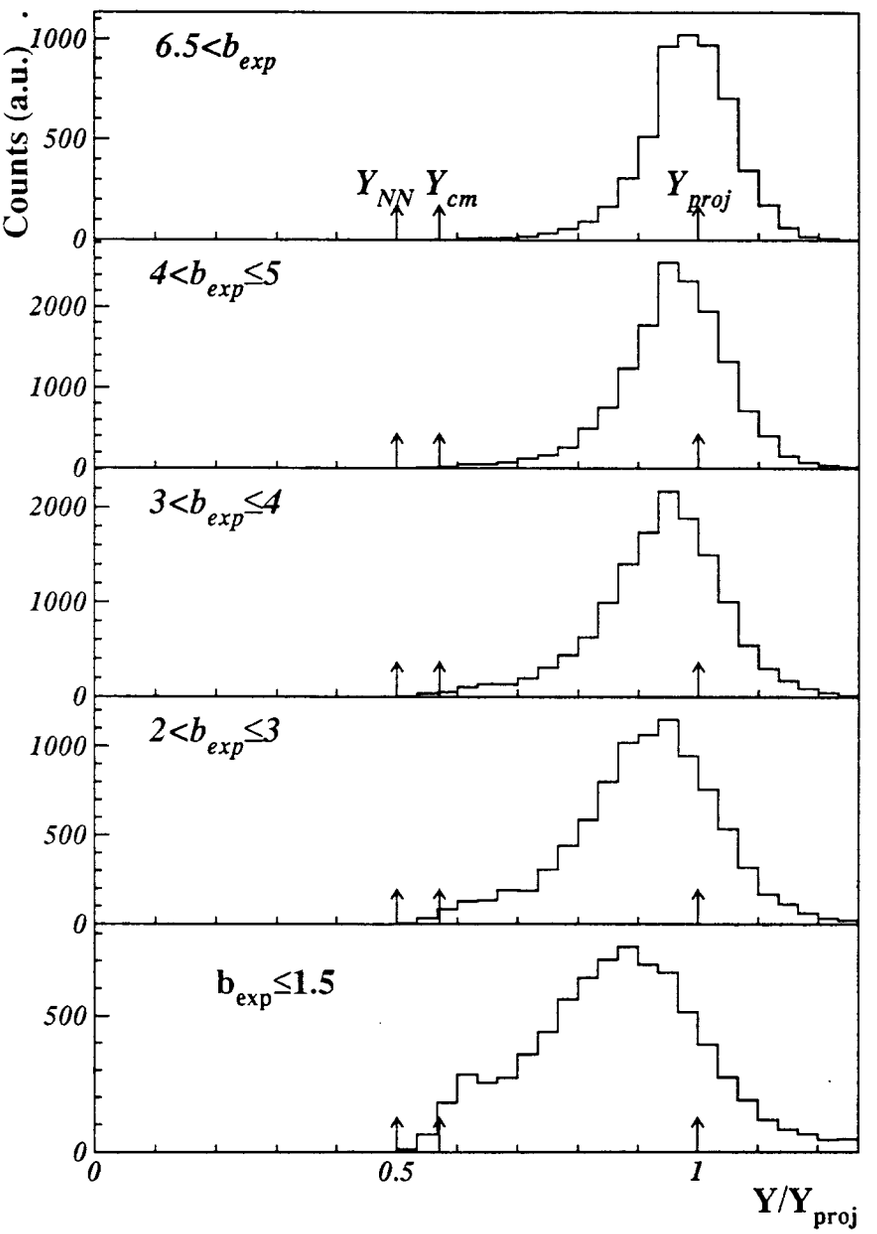

8 - Rapidity distributions (normalized to the projectile rapidity) of Z=6-9, respectively for five impact parameter bins at 67 MeV/u. The impact parameter sorting is made with the sum of transverse momenta, $P_{\perp}$.

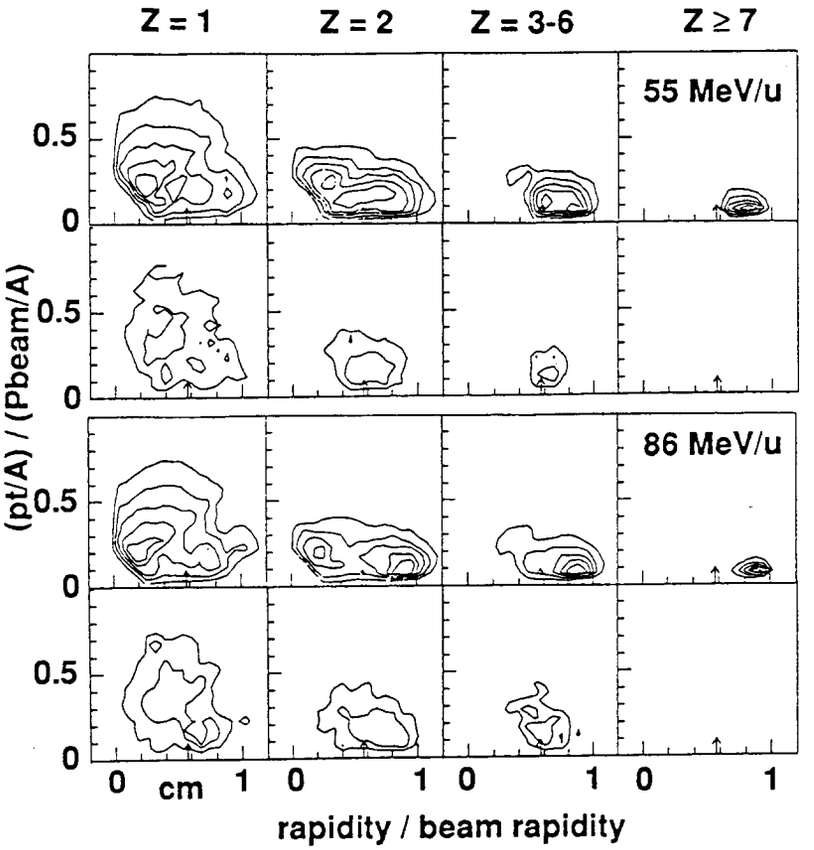

9 - Contour plots for Z=1, 2, 3-6 and ≥ 7 at 55 (top) and 86 MeV/u (bottom). At each energy, the upper row contains all events with an estimated impact parameter ≤ 1 fm , the lower row contains the events of the upper row which have a large $E_{\perp}$ / $E_{//}$ ratio, i.e. possible fusion events (see text). The abcissa is the laboratory rapidity normalized to the projectile rapidity and the ordinate is the transverse momentum per nucleon relative to the projectile momentum per nucleon.

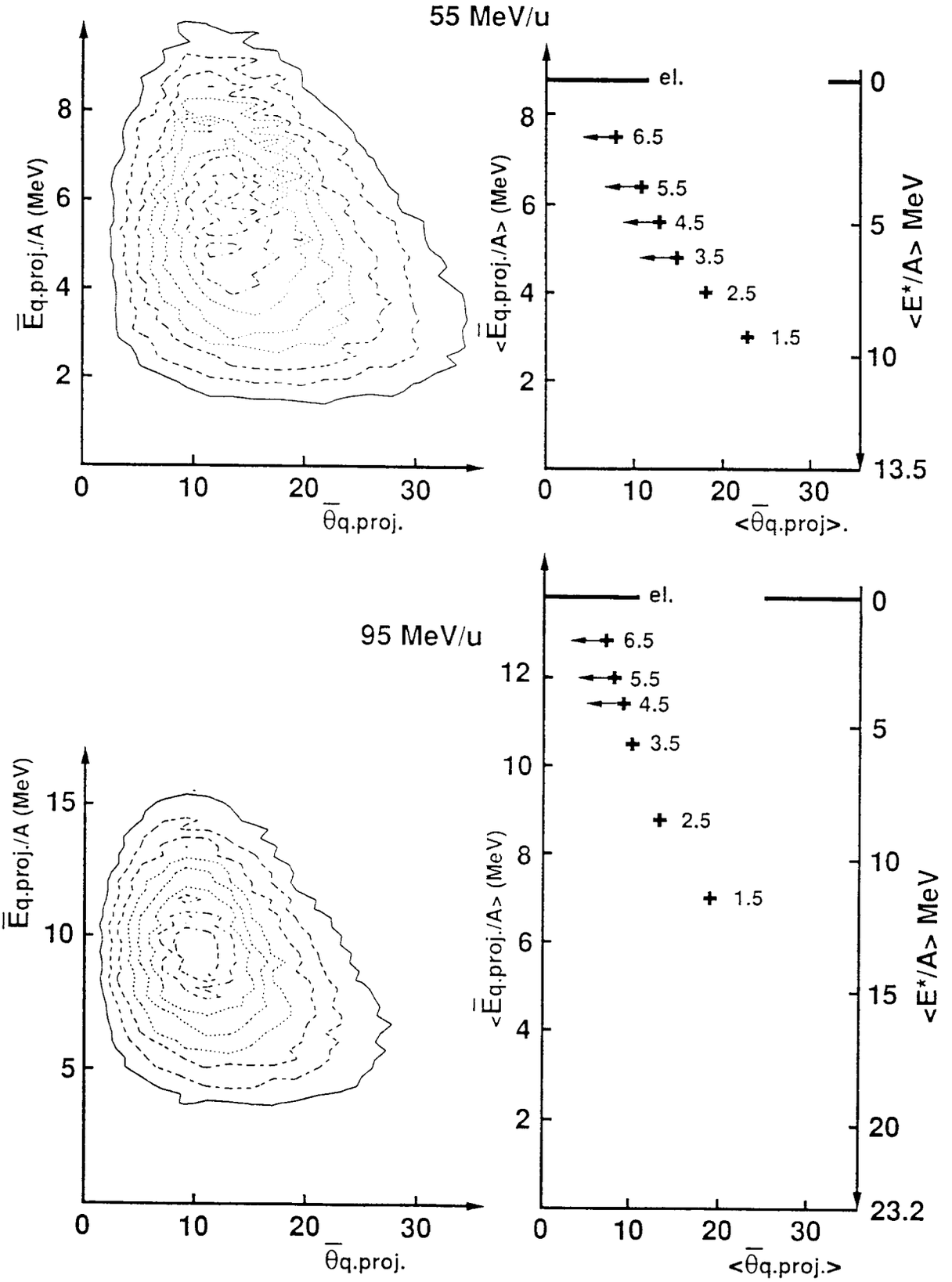

10 - Left top panel : contour plots of the c.m. kinetic energy per nucleon of the reconstructed quasi-projectile versus its c.m. deflection angle (bounce-off angle) at 55 MeV/u. Right top panels : mean values of the same observables per b_{exp} bin. The label 1.5 means : b_{exp} = 0 to 1.5 fm, 2.5 means from 1.5 to 2.5 fm, and so on. The right-hand vertical scale is the corresponding dissipated energy per nucleon. Bottom panels : same as top panels, but at 95 MeV/u.

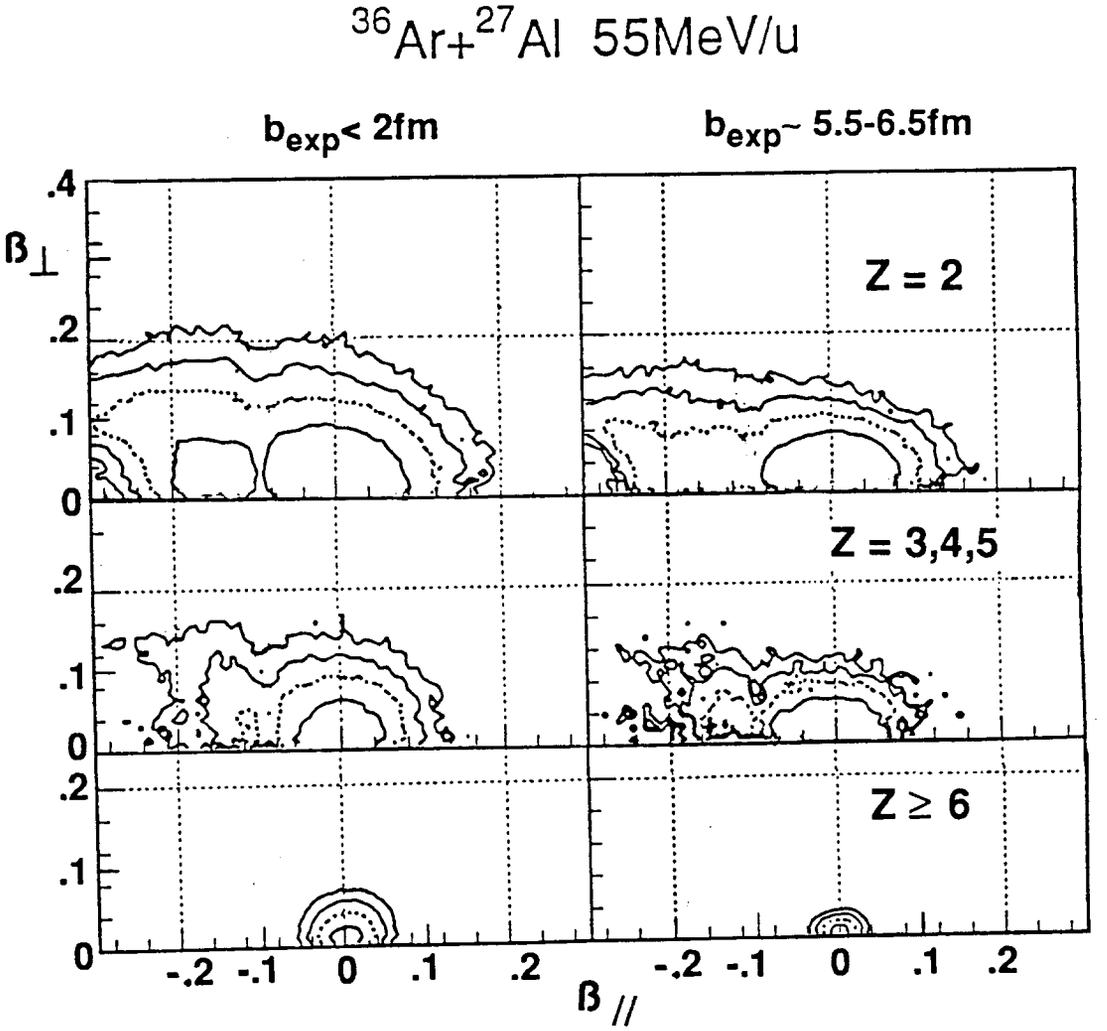

11 - Lorentz invariant cross sections in the reference frame of the quasi-projectile at 55 MeV/u . *Left side panels* : central collisions (b_{exp} < 2 fm). *Right side panels* : semi-peripheral collisions (b_{exp} = 5.5 - 6.5 fm). Bottom : heavy products (Z ≥ 6) ; middle : Z=3, 4, 5 ; top : Z=2 .

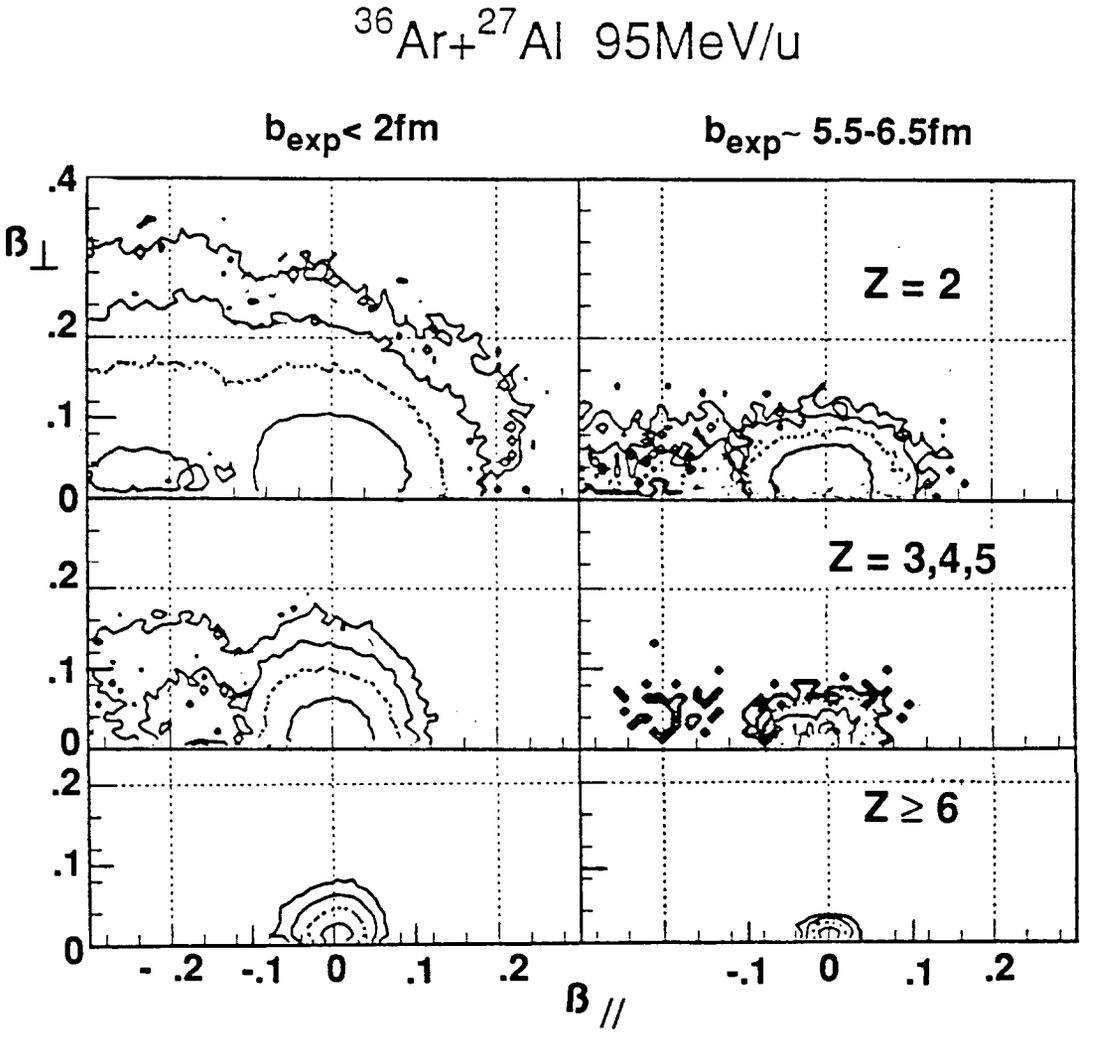

12 - Same as fig. 11, but at 95 MeV/u .

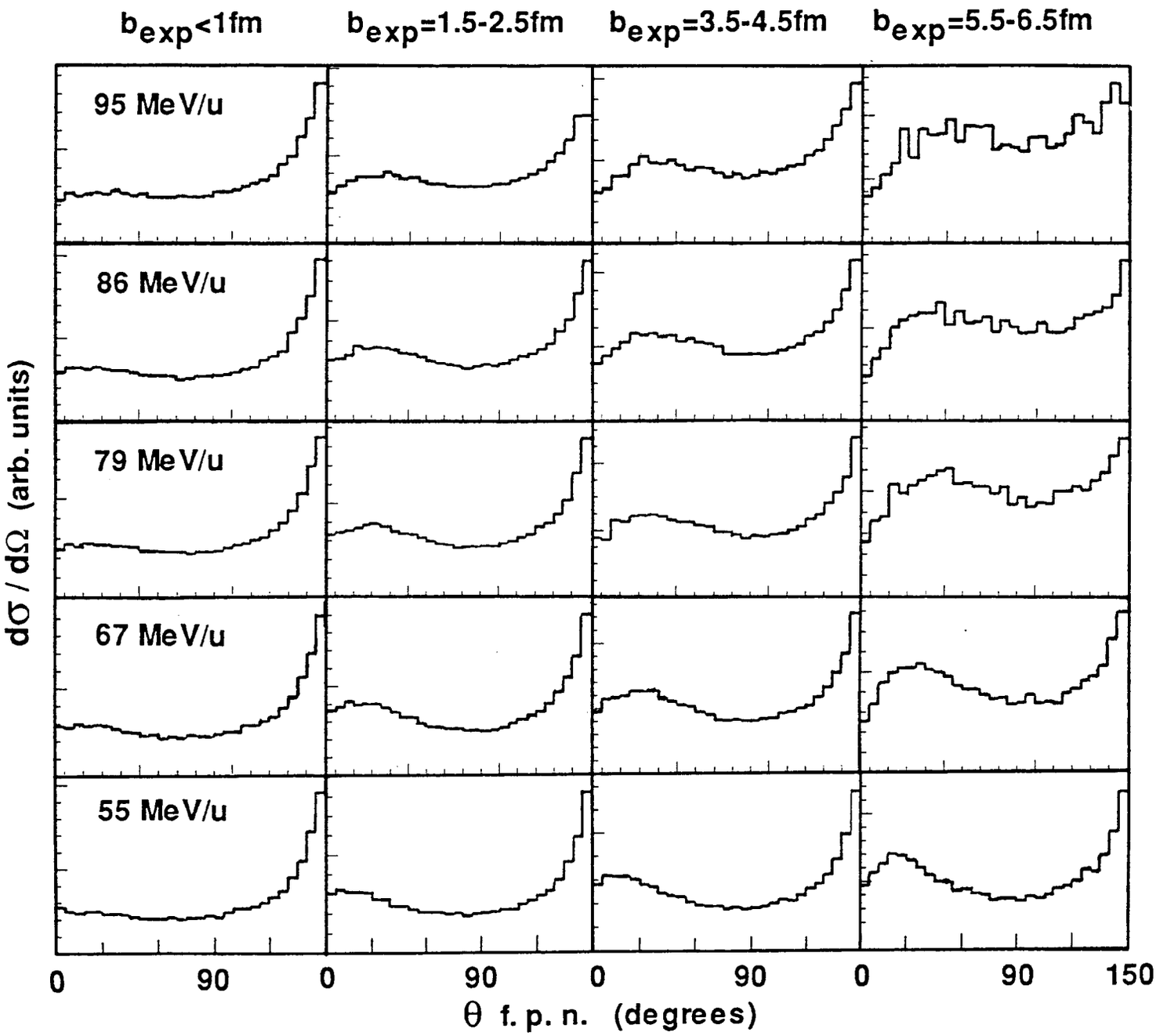

13 - Angular distributions dN / dΩ of Z=2 particles (mostly a particles) in the frame of the quasi-projectile. From bottom to top : 55, 67, 79, 86 and 95 MeV/u . *From left to right* : central (b_{exp} < 1.0 fm), semi-central (b_{exp} = 1.5 - 2.5 fm), intermediate (b_{exp} = 3.5 - 4.5 fm) and semi-peripheral (b_{exp} = 5.5 - 6.5 fm) collisions. The decrease near 0° is due to the hole in MUR at forward laboratory angles (see text). The increase at backward angles is due to the contributions from mid-rapidity particles and target-like (slow source) emission.

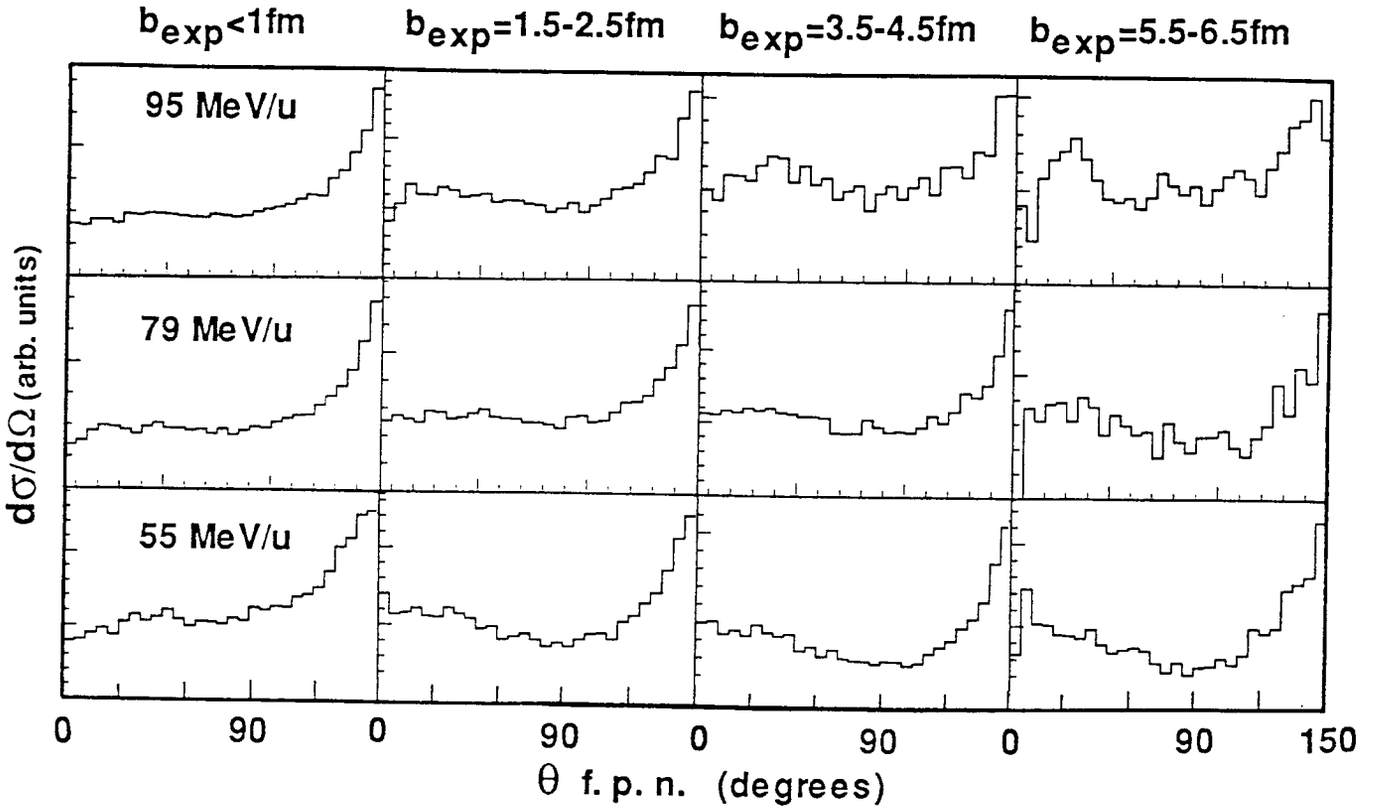

14 - Same as fig. 13, for IMF's with Z=3, 4, 5 .

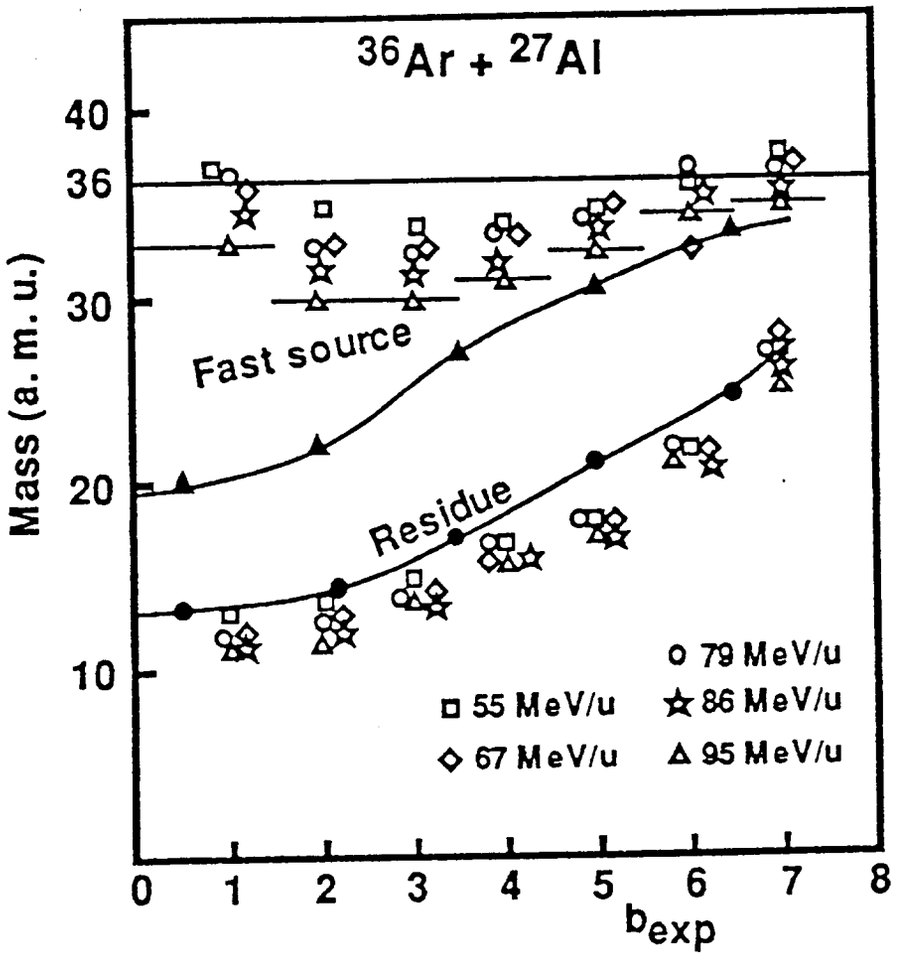

15 - Experimental data and Landau-Vlasov calculations as a function of the impact parameter. The experimental data are shown by open symbols. In each figure, the lower points show the mean residual mass of the quasi-projectile, the upper points show the mean reconstructed mass of the quasi-projectile. The reconstructed mass includes some pre-equilibrium contribution, especially in central collisions. The horizontal bars show the estimated impact parameter bins. Landau-Vlasov calculation results at 65 MeV/u for Ar+Al and 62 MeV/u for Zn+Ti are shown by closed symbols. Points : average residual mass of the fast source ; triangles : average mass of the fast source at the moment of separation from the slow source.

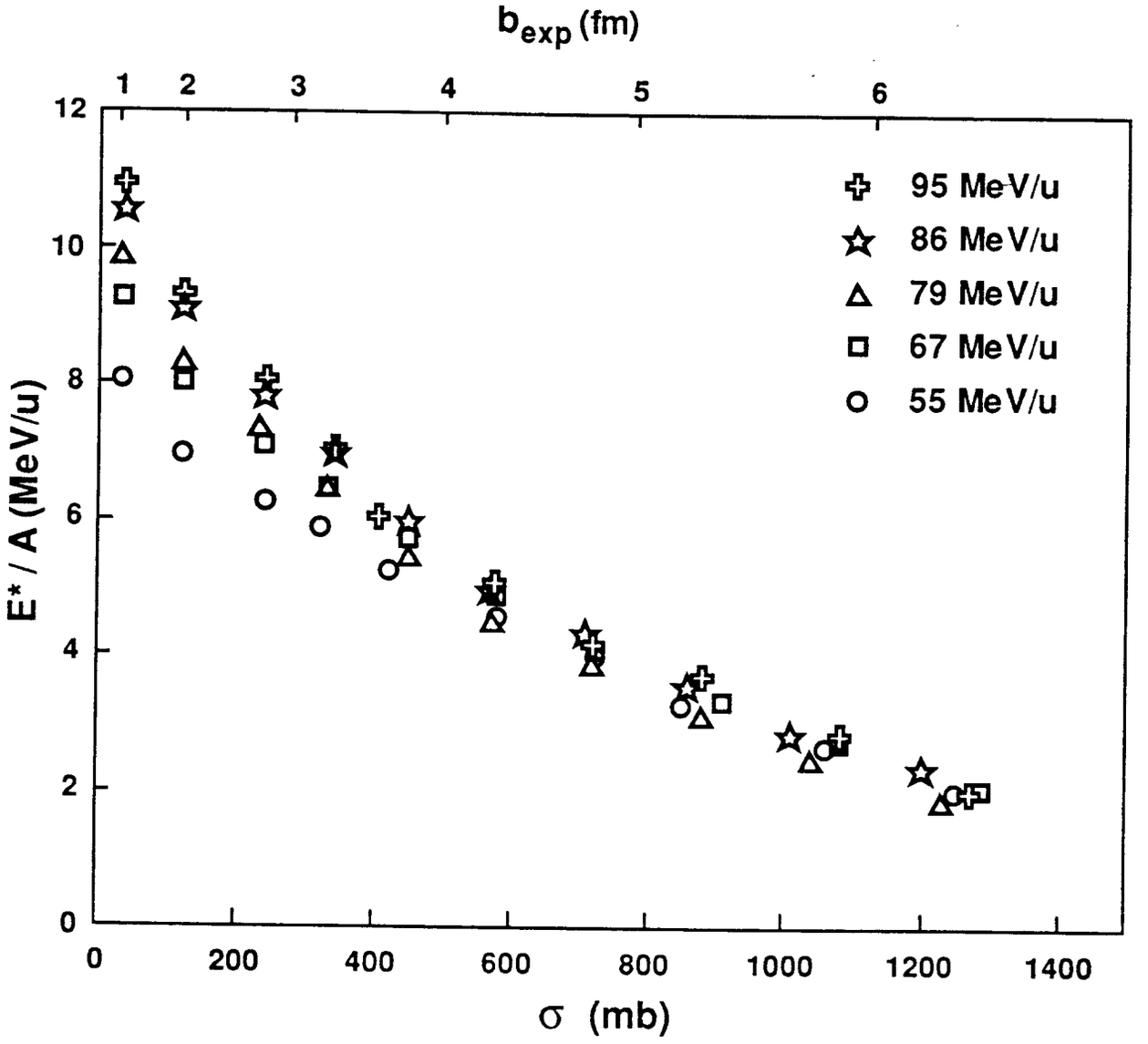

16 - Mean excitation energy per nucleon of the quasi-projectile in each impact parameter bin at the five incident energies. Grazing collisions occur at 8 fm (~2000 mb).

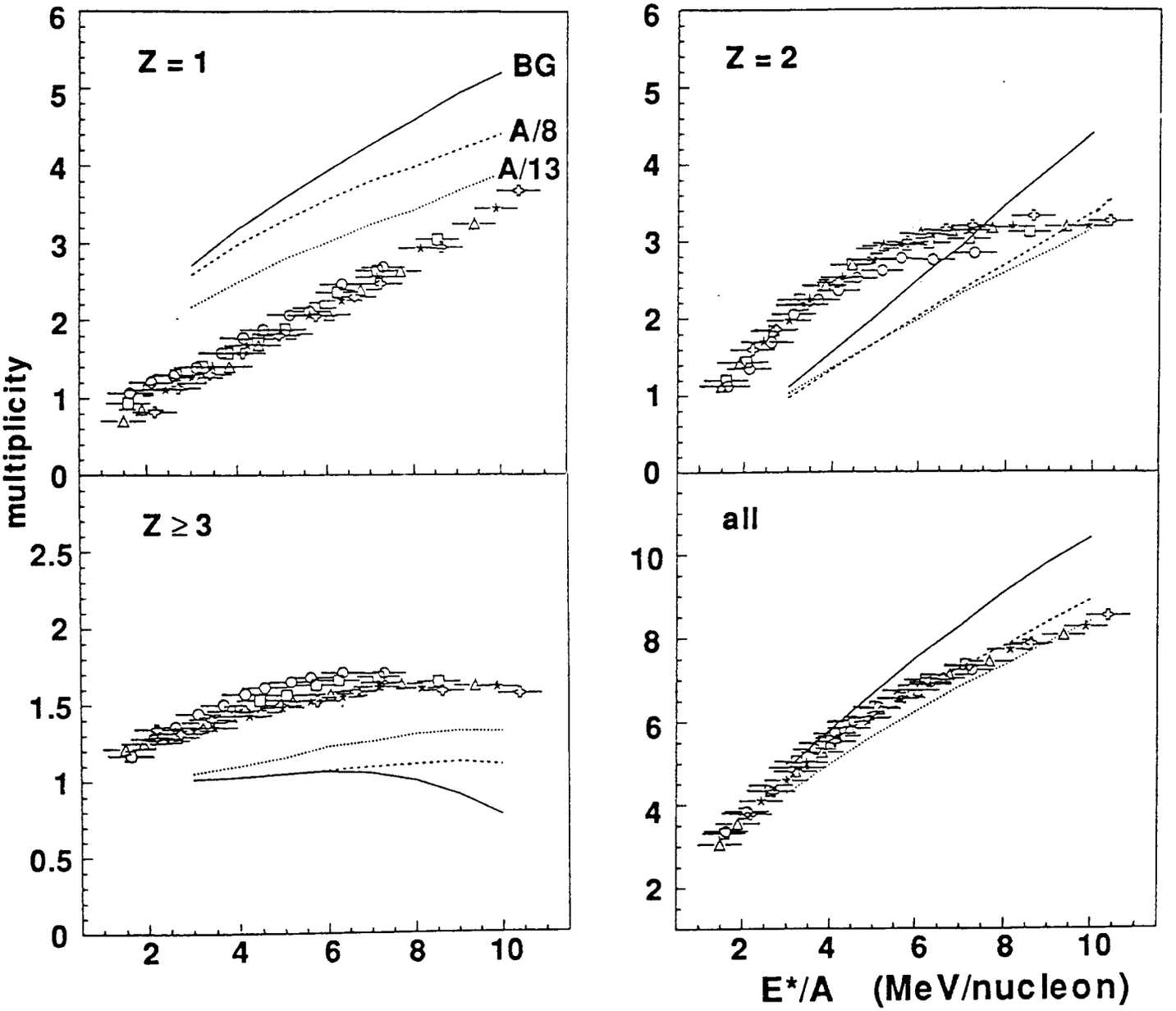

17 - Mean multiplicity of products from the quasi-projectile versus its excitation energy per nucleon. The symbols corresponding to the five incident energies are the same as in fig. 14. The lines were obtained from a sequential de-excitation code with a constant level density parameter set equal to A/8 (dashed lines) or A/8 (dotted lines) or according to ref. [27] (solid lines).

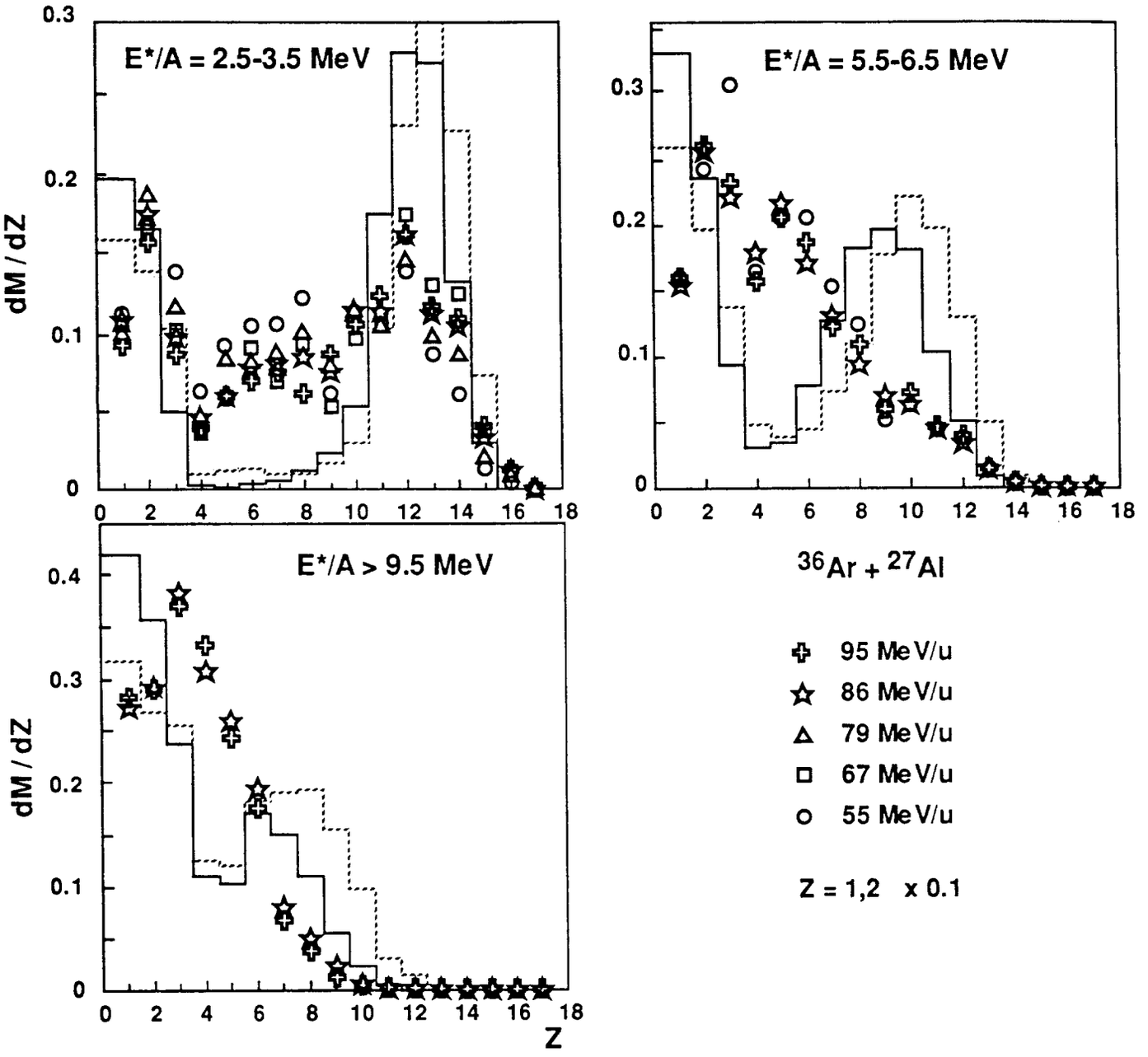

18 - Charge distributions (average multiplicities) of products from the quasi-projectile (fast source) for three bins of excitation energy per nucleon. Points : experimental data. Lines : calculation with statistical sequential emission ; solid lines : with the level density of ref. [27] ; dashed lines : with a constant level density parameter a = A/13 .

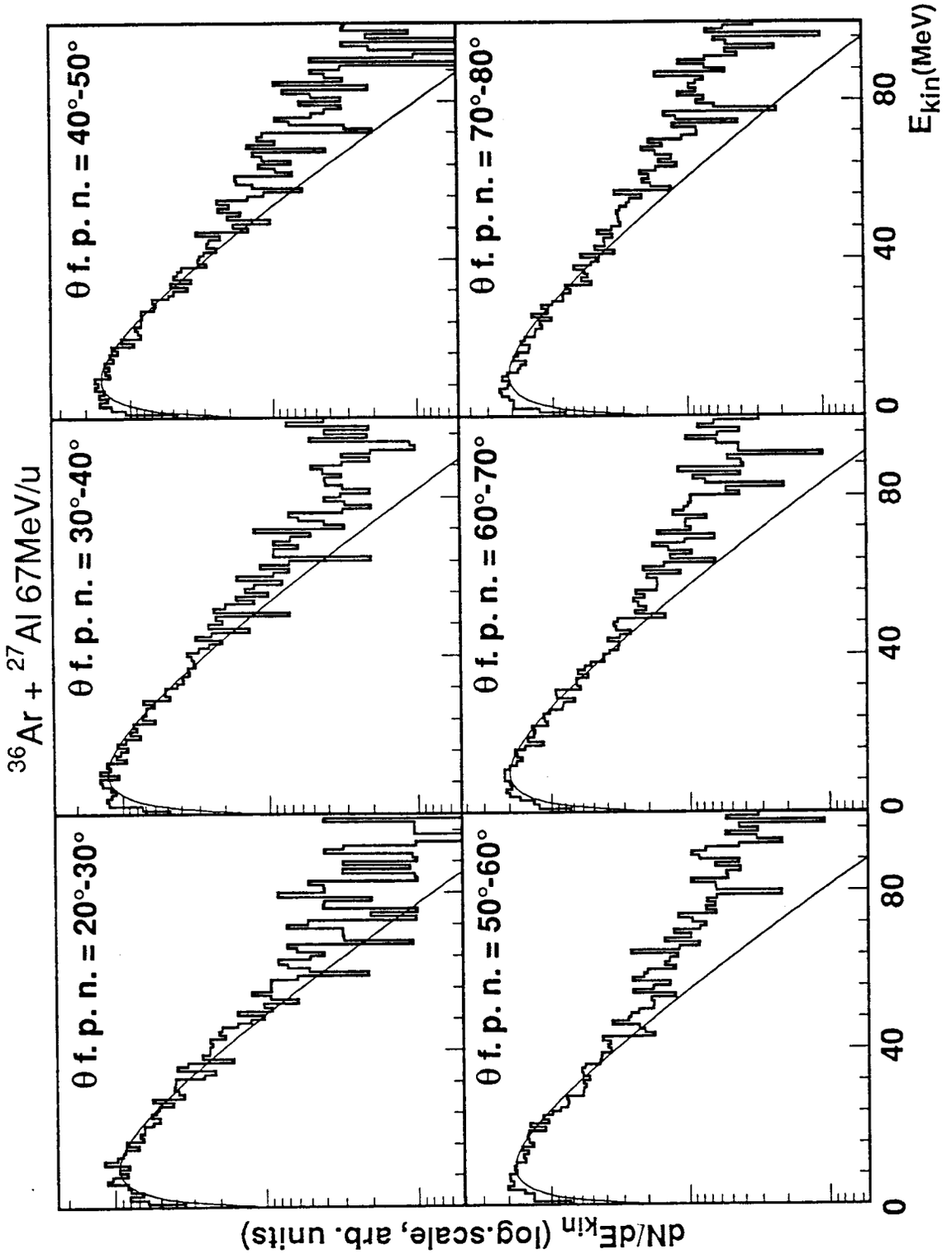

19 - Kinetic energy distribution for Z=2 particles in the rest frame of the quasi-projectile at various angular bins in this frame.

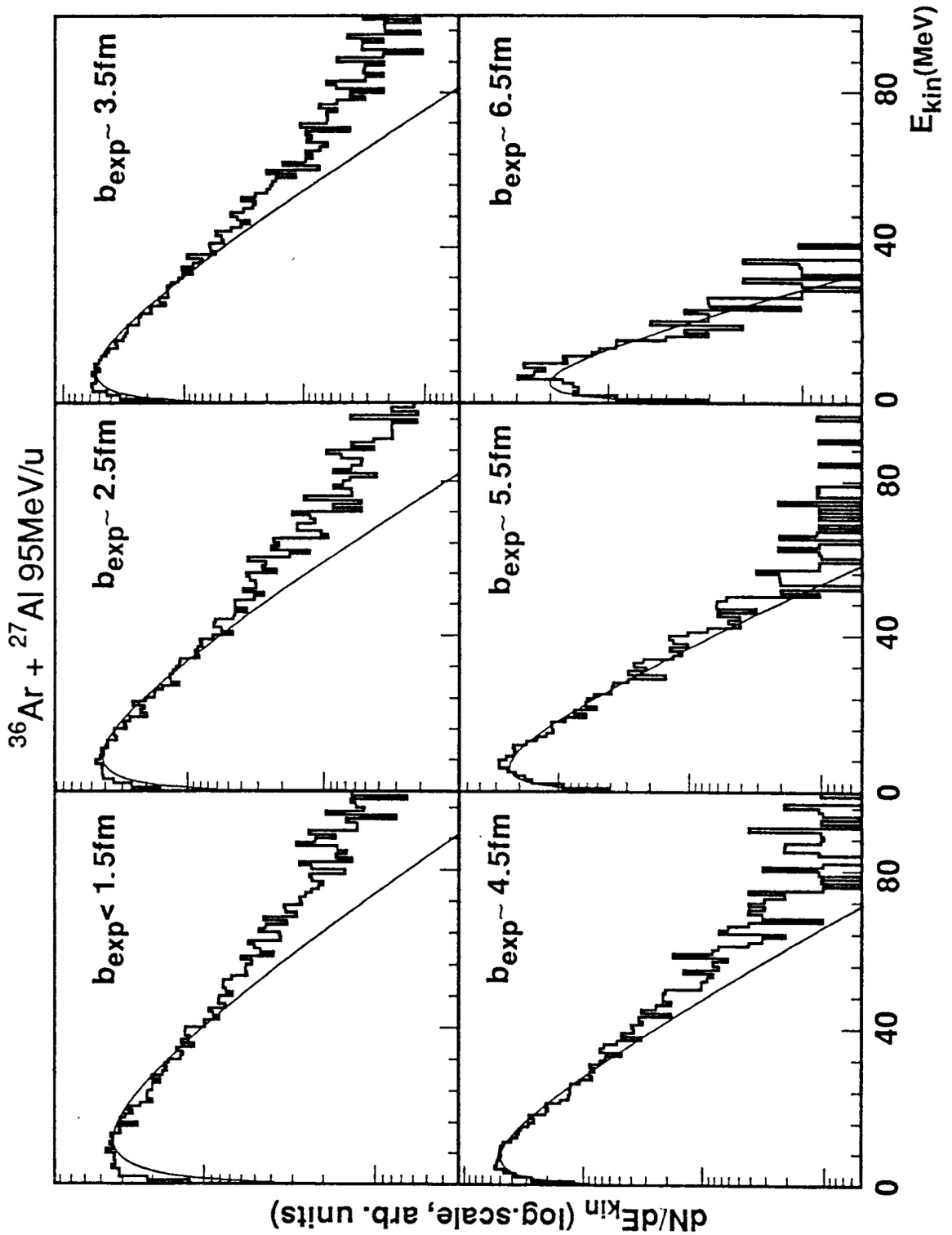

20 - Kinetic energy distributions for Z=2 particles at 30-60° in the rest frame of the quasi-projectile at 95 MeV/u for different impact parameters. The solid line represents the fit used to determine the slope parameter.

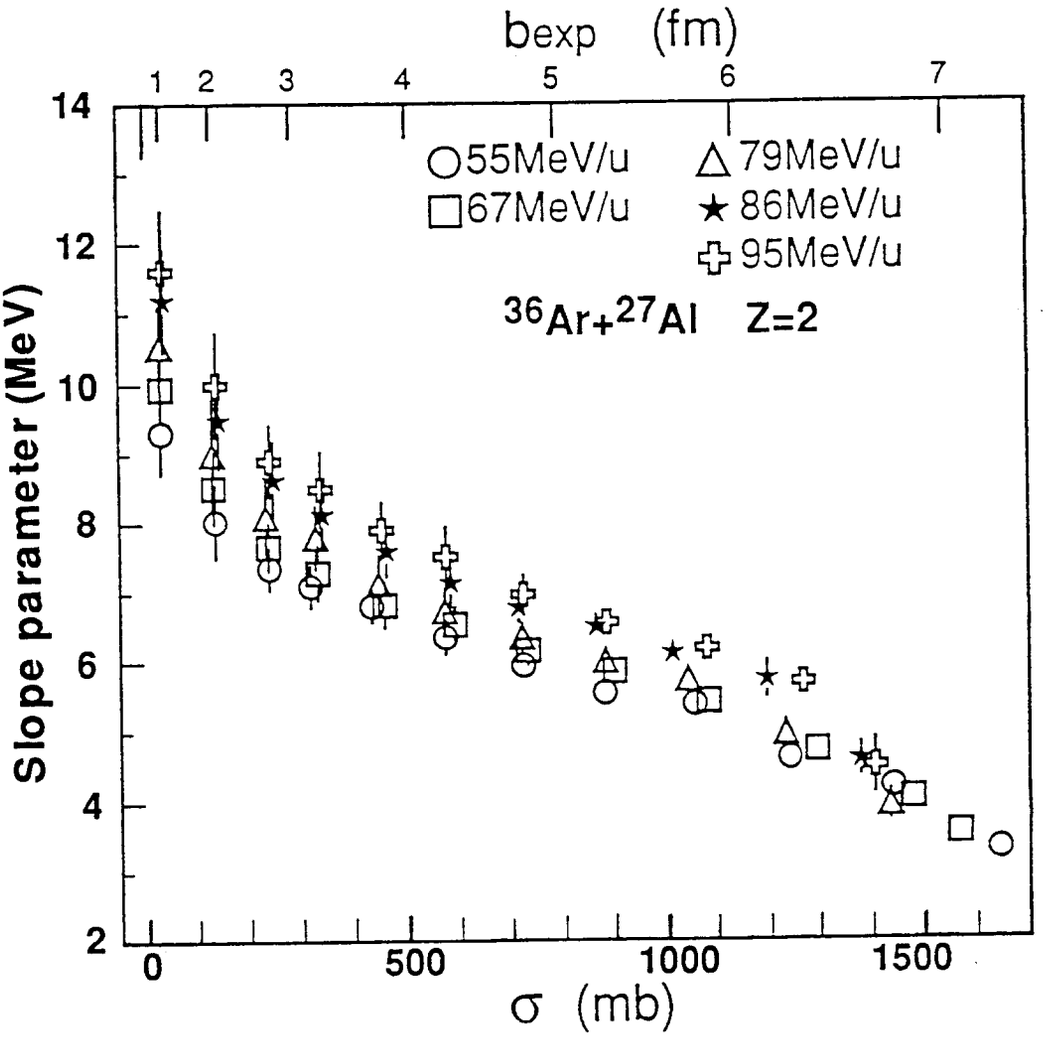

21 - Slope parameter of the kinetic energy distributions of Z=2 particles as a function of the impact parameter (top scale) at incident energies 55, 67, 79, 86 and 95 MeV/u. For clarity not all error bars are drawn. The grazing impact parameter value is ~8 fm . The bottom scale represents the cross section integrated from $b_{exp} = 0$ to b_{exp} .

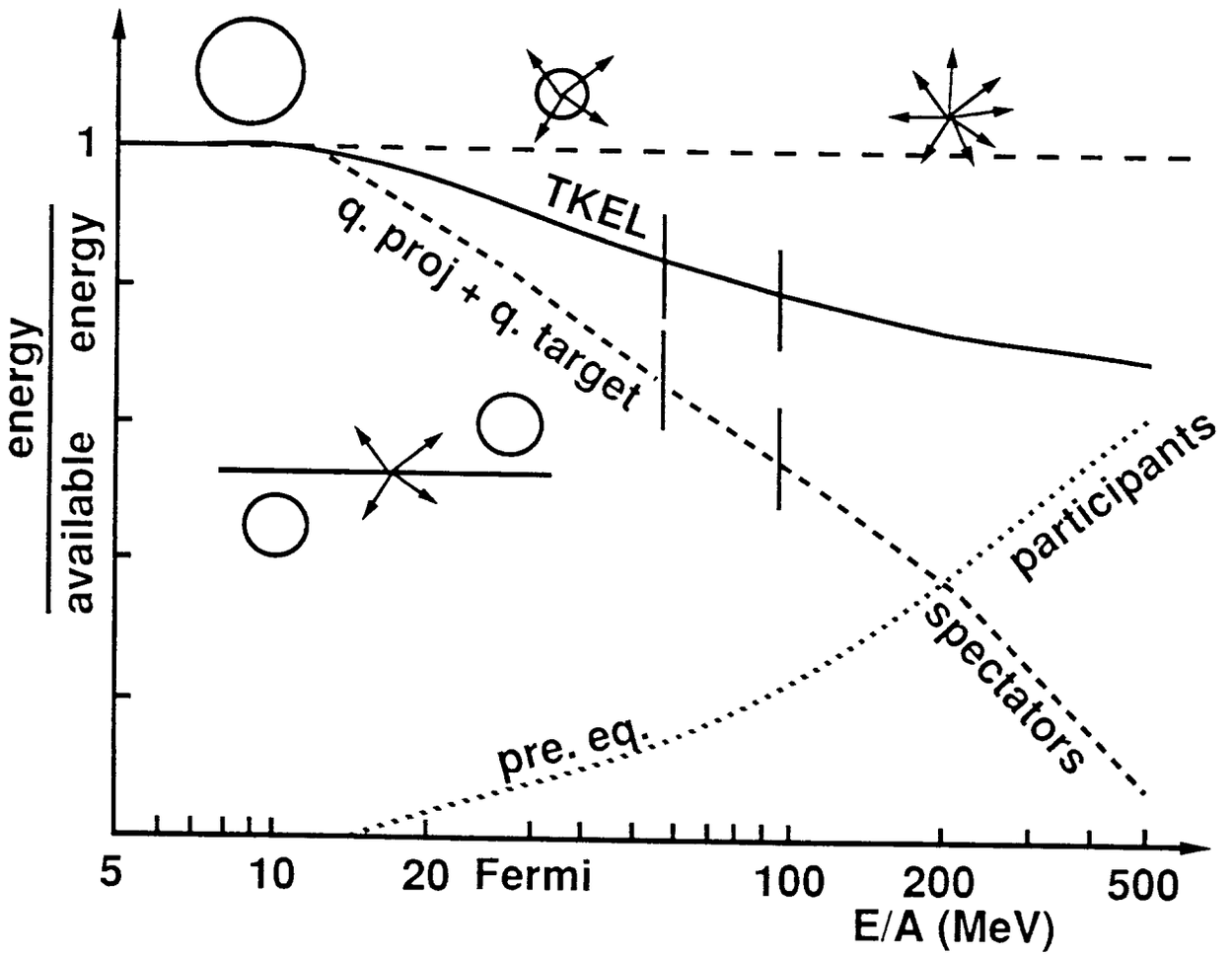

22 - Schematic picture of the evolution of reaction mechanisms with incident energy. Long dashed line : single source events (fusion or full stopping). Other lines : central collisions (<4 % σ_R). Solid line : Total Kinetic Energy Loss TKEL (dissipated energy). Dotted line : total energy of particles emitted from the interaction zone (pre-equilibrium particles, or participants). Short dashed line : excitation energy of the quasi-projectile + quasi-target, or spectators.